



Published in final edited form as:

Cell Rep. 2022 December 13; 41(11): 111827. doi:10.1016/j.celrep.2022.111827.

EGFR-phosphorylated GDH1 harmonizes with RSK2 to drive CREB activation and tumor metastasis in EGFR-activated lung cancer

JiHoon Kang^{1,7}, Jaemoo Chun^{1,7}, Jung Seok Hwang¹, Chaoyun Pan¹, Jie Li¹, Austin C. Boese¹, Isabelle Young¹, Courteney M. Malin¹, Yibin Kang², Don L. Gibbons³, Gabriel Sica⁴, Haian Fu⁵, Suresh S. Ramalingam¹, Lingtao Jin^{6,*}, Sumin Kang^{1,8,*}

¹Department of Hematology and Medical Oncology, Winship Cancer Institute of Emory, Emory University School of Medicine, Atlanta, GA 30322, USA

²Department of Molecular Biology, Princeton University, and Ludwig Institute for Cancer Research Princeton Branch, Princeton, NJ 08544, USA

³Department of Thoracic-Head and Neck Medical Oncology, the University of Texas MD Anderson Cancer Center, Houston, TX 77030, USA

⁴Department of Pathology and Laboratory Medicine, Emory University School of Medicine, Atlanta, GA 30322, USA

⁵Department of Pharmacology and Chemical Biology, Emory University School of Medicine, Atlanta, GA 30322, USA

⁶Department of Molecular Medicine, UT Health San Antonio, San Antonio, TX 78229, USA

⁷These authors contributed equally

⁸Lead contact

SUMMARY

The cancer metastasis process involves dysregulated oncogenic kinase signaling, but how this orchestrates metabolic networks and signal cascades to promote metastasis is largely unclear. Here we report that inhibition of glutamate dehydrogenase 1 (GDH1) and ribosomal S6 kinase 2 (RSK2) synergistically attenuates cell invasion, anoikis resistance, and immune escape in lung cancer and more evidently in tumors harboring epidermal growth factor receptor (EGFR)-activating or EGFR inhibitor-resistant mutations. Mechanistically, GDH1 is activated by EGFR

This is an open access article under the CC BY-NC-ND license (<http://creativecommons.org/licenses/by-nc-nd/4.0/>).

*Correspondence: jinl1@uthscsa.edu (L.J.), smkang@emory.edu (S.K.).

AUTHOR CONTRIBUTIONS

D.L.G., Y.K., H.F., and S.R. provided critical reagents. G.S. conducted histopathological analyses. I.Y. established metabolic inhibitor library. J.C. performed bioluminescence imaging and CaMKIV activity assay. L.J. conducted α -KG rescue experiment. C.P. and J.L. conducted part of the study related to EGFR-GDH1 link. J.K., J.S.H., A.C.B., and C.M.M. performed all other experiments. L.J. and S.K. designed the study, and J.K. and S.K. wrote the paper.

DECLARATION OF INTERESTS

The authors declare no competing interests.

SUPPLEMENTAL INFORMATION

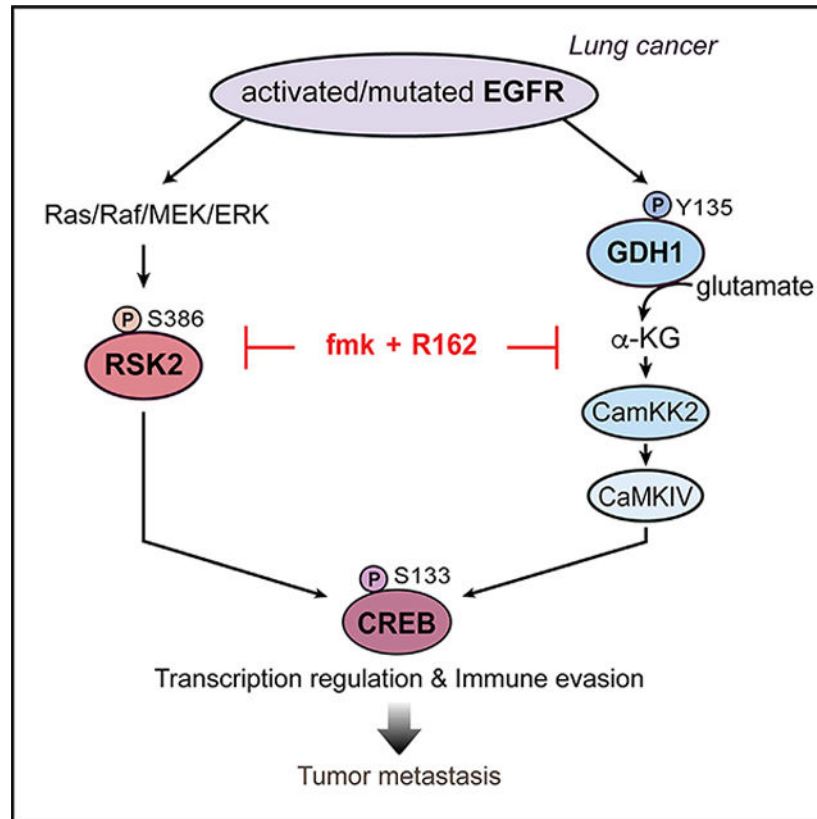
Supplemental information can be found online at <https://doi.org/10.1016/j.celrep.2022.111827>.

through phosphorylation at tyrosine 135 and, together with RSK2, enhances the cAMP response element-binding protein (CREB) activity via CaMKIV signaling, thereby promoting metastasis. Co-targeting RSK2 and GDH1 leads to enhanced intratumoral CD8 T cell infiltration. Moreover, GDH1, RSK2, and CREB phosphorylation positively correlate with EGFR mutation and activation in lung cancer patient tumors. Our findings reveal a crosstalk between kinase, metabolic, and transcription machinery in metastasis and offer an alternative combinatorial therapeutic strategy to target metastatic cancers with activated EGFRs that are often EGFR therapy resistant.

In brief

Although oncogenic kinases are associated with human cancers, how they manage metabolic networks and cellular signaling to promote metastasis remains unclear. In this article, Kang et al. demonstrate a mechanism by which EGFR-activated GDH1 and RSK2 are intertwined to enhance CREB transcription activity and promote tumor metastasis in lung cancer.

Graphical Abstract



INTRODUCTION

Cancer cells have a large spectrum of metastasis-related mechanisms tightly controlled by several signaling factors, and a single agent is often insufficient to target metastasis.¹ Considering the complexity of the metastatic process, there is an urgent need to understand and identify a potent combined therapeutic strategy to overcome metastasis.

Protein kinases orchestrate the activation of pro-survival signaling cascades that drive cancer progression.² Overexpression and activating mutations of epidermal growth factor receptor (EGFR) frequently occur in human cancers, including non-small cell lung carcinoma (NSCLC) and head and neck squamous cell carcinoma, and have been a critical therapeutic target for the treatment of these tumors.^{3–5} Recent clinical trials showed that the third-generation EGFR inhibitor osimertinib has prominently improved efficacy in progression-free survival compared with first-generation EGFR inhibitors erlotinib and gefitinib in NSCLC.⁶ Despite high tumor response rates, most patients eventually develop resistance to treatment and have cancer progression following EGFR inhibitor treatment.

EGFR aberrations activate downstream pro-oncogenic signaling pathways, including the MAPK pathway, which is activated by multiple effectors, including G-protein-coupled receptors and the kinase Src.⁷ P90 ribosomal S6 kinase 2 (RSK2) is a serine/threonine kinase downstream of ERK in the MAPK pathway that phosphorylates multiple signaling effectors, including histone H3, Myt1, BAD, and BIM, to regulate transcriptional machinery, cell cycle, and survival.⁸ RSK2 plays a critical role in promoting multiple steps of tumor metastasis, including invasion, migration, and resistance to detachment-induced cell death (a.k.a. anoikis^{9–11}) by phosphorylating a spectrum of protein factors, including ASK1, Hsp27, and stathmin in human cancers.¹² RSK2 phosphorylates cAMP response element-binding protein (CREB) at S133 and consequently modulates the gene expression of anti- or pro-apoptotic factors, including PTK6 and ING3, to confer anoikis resistance to cancer cells.¹² In addition, studies have revealed a specific function of CREB in the immune response that involves cytokine expression and NF- κ B activation.¹³ The RSK-specific inhibitor fmk and its derivative fmk-MEA, as well as 666–15 that specifically targets CREB, are known to effectively attenuate tumor growth and metastasis in mice.^{14,15}

Accumulating evidence suggests that reprogrammed cellular metabolism is an emerging hallmark of cancers.^{16–21} Glutaminolysis is a metabolic pathway that converts glutamine into glutamate and consequently alpha-ketoglutarate (α -KG) and ammonia.²² Elevated glutaminolysis in cancer cells has been theoretically justified.²³ Studies suggest that inhibition of glutaminase (GLS), the first enzyme in the glutaminolysis pathway that converts glutamine to glutamate, using GLS inhibitors effectively attenuates tumor growth.^{24–26}

Glutamate dehydrogenase 1 (GDH1), the second enzyme in the glutaminolysis pathway, and its product α -KG contribute to energy production by activating AMPK to promote anoikis resistance and tumor metastasis in lung cancer.²⁷ Mechanistically, GDH1 activates CamKK2 by GDH1 product α -KG binding to CamKK2 and recruiting its substrate AMPK to CamKK2, which consequently triggers AMPK signaling and promotes energy production that confers metastatic potential.²⁷ Farris et al. found that GDH1 and α -KG are enhanced during the epithelial-to-mesenchymal transition (EMT) and are critical for suppressing reactive oxygen species (ROS) and consequently protecting epithelial cells against anoikis.^{28,29} These findings imply that the role of α -KG in cell metabolism may depend on cell type and discrete cellular metabolic conditions. Targeting GDH1 with the GDH1-specific small molecule inhibitor R162 decreased tumor growth.³⁰

Although both protein kinases and metabolic factors are critical in promoting tumor progression, the detailed mechanisms by which these two distinct signaling pathways are intertwined to drive tumor progression are largely unclear. Here we report the mechanism by which these two distinct signaling axes involving RSK2 and GDH1 are activated by EGFR to coordinately provide the pro-metastatic potential to cancer cells and functionally evaluate the therapeutic efficacy of targeting these two factors in combination in advanced EGFR-driven cancers.

RESULTS

Dual inhibition of GDH1 and RSK2 synergistically suppresses invasion and sensitizes cancer cells to anoikis induction

To better understand the crosstalk between metabolic pathways and cellular kinase signaling in cancer metastasis, we generated a customized metabolic inhibitor library that consists of compounds targeting a panel of cancer-related metabolic enzymes and examined their effect in combination with fmk, an inhibitor of the pro-metastatic kinase RSK2, on invasion inhibition and anoikis induction (Table S1). Among 14 metabolic inhibitors tested, combined treatment with R162, the GDH inhibitor, and fmk was identified to be the most effective combination to inhibit invasion and promote anoikis (Figure 1A). To confirm the screening results, we first validated the effect of targeting GDH1 and RSK2 in combination in a group of human cell lines, including A549 and H157 lung cancer cells and non-malignant fetal lung fibroblast MRC-5 and lung epithelial BEAS-2B. Combined treatment with both agents significantly further reduced invasion, migration, and anoikis resistance with combination index (CI) values of 0.44~0.66 in cancer cells, whereas the combination did not alter these potentials in control normal proliferating cells (Figures 1B and 1C). Similar results were obtained when RSK2 and glutaminase-GDH1 signaling were pharmacologically targeted with inhibitors other than fmk and R162 (Figures S1A–S1D). In addition, the R162 or fmk effect was abolished in cells lacking GDH1 or RSK2, suggesting that the effects occurred by specifically targeting GDH1 or RSK2 (Figures S1E and S1F).

Moreover, genetic inhibition of RSK2 and GDH1 using their specific shRNA clones further decreased invasion and migration and sensitized cells to anoikis compared with cells with a single knockdown (Figure 1D). We further validated the effect of targeting RSK2 and GDH1 on tumor metastasis *in vivo* using a xenograft mouse model of lung cancer. Targeting both GDH1 and RSK2 by either knockdown or inhibitor treatment did not cause any noticeable damage to diverse organs but resulted in significantly decreased metastatic potential compared with the group targeting either one (Figures 1E, 1F, and S1G–S1L). These data suggest that a glutaminolytic enzyme GDH1 and a kinase RSK2 play a coordinating role in promoting tumor metastasis in lung cancer.

GDH1 and RSK2 signaling converge on the transcription factor CREB to promote metastasis

To elucidate the molecular mechanism by which GDH1 and RSK2 cooperate to promote tumor metastasis, we first surveyed potential links to metabolism. Although metabolic changes, including decreased glutaminolysis rate, elevated ROS, and attenuated cellular

energetics, were induced by GDH1 inhibition, dual targeting of GDH1 and RSK2 did not further impact these changes, suggesting that these two factors do not potentiate metastasis through metabolic rearrangements (Figures S2A–S2D).

To comprehensively gain mechanistic insight into how these two distinct signaling axes intersect, we performed a phosphorylation pathway profiling. We monitored the phosphorylation of 55 factors in pathways that control cellular events, including MAPK, AKT, JAK/STAT, NF- κ B, and TGF- β in lung cancer cells with dual knockdown of GDH1 and RSK2. A decrease in p53 phosphorylation was observed at S15 in the phosphorylation pathway profiling, which is the site known to correspond to elevation of p53 activity as a tumor suppressor, suggesting that this change is the consequence of cells attempting to compensate and survive the GDH1 and RSK2 loss. We observed that the MAPK pathway, in particular the phosphorylation of CREB at serine 133, which is known to enhance its transcription activity, was further decreased when A549 cells lacked both GDH1 and RSK2 (Figure 2A). The array results were confirmed by immunoblotting, which showed that genetic downregulation of GDH1 and RSK2 mediated decreased phosphorylation and activation of CREB (Figures 2B and 2C). In addition, the expression levels of CREB targets including Fascin-1 and PTK6 aligned with CREB activity, whereas mRNA levels of ING3, for which CREB functions as an inhibitory regulator, were further increased when cells lacked both RSK2 and GDH1 (Figure 2D). Similar results were obtained when alternative shRNA clones or inhibitors were used to target RSK2 and GDH1 (Figures S3A–S3E and S4A–S4C). Furthermore, phospho-mimetic CREB mutant S133D, but not phospho-deficient CREB mutant S133A, significantly rescued the decreased cell invasion and anoikis resistance seen in GDH1 and RSK2 double-knockdown cells (Figure 2E). An additional potential downstream target, p38, from the profiling was identified to be the upstream factor of CREB by inhibitor analysis (Figure 2F). However, simultaneous reactivation of CREB and p38 did not further reverse the enhanced anoikis and decreased invasion mediated by RSK2 and GDH1 loss, compared with RSK2/GDH1 inhibition with the single rescue of CREB S133D (Figures 2G and 2H). Collectively, these data demonstrate that GDH1 and RSK2 signaling mainly converge on CREB to promote cancer cell invasion and anoikis resistance.

GDH1/RSK2-CREB signaling is critical for invasion in EGFR mutant cancer

To explore a cancer population that primarily depends on GDH1/RSK2-CREB signaling for invasion, we examined the effect of targeting RSK2 and GDH1 in combination or CREB in a panel of lung cancer cells with diverse oncogenic driver mutations including NRas/KRas, BRaf, EGFR, CDKN2A, PI3KCA, P53, and LKB1.³¹ Among 12 lung cancer cell lines tested, the group of cells harboring EGFR-activating or EGFR inhibitor-resistant mutations was more sensitive to GDH1 and RSK2 inhibition compared with the group of cells with EGFR wild type (WT) and mutations in other factors (Figure 3A). In line with this observation, pharmacological or genetic inhibition of CREB, the mutual target of RSK2 and GDH1, diminished invasive potential in EGFR mutant cells at a greater level compared with cells that harbor EGFR WT (Figures 3B and 3C). These data suggest that the GDH1/RSK2-CREB signaling axis is pivotal for EGFR-mutated cancer cell invasion.

We next compared the effect of targeting the GDH1/RSK2-CREB axis or EGFR with sublethal doses of GDH/RSK, CREB, or EGFR inhibitors on cell invasion in patient-derived tumors with different EGFR status. Although the efficacy varied among tumors, targeting RSK2/GDH1-CREB or EGFR was similarly effective in attenuating invasion in EGFR WT tumors. In contrast, targeting the GDH1/RSK2-CREB axis was more effective than targeting EGFR when tumors had EGFR-activating and/or inhibitor-resistant mutations (Figure 4A; Table S2). We further validated our finding in sets of lung cancer cell lines that are resistant to EGFR inhibitors. These cells were 1,513~3,212 times more resistant to erlotinib or osimertinib compared with parental HCC827 and PC9 cells (Figures S5A–S5D). Consistent with the observation in patient-derived tumors with EGFR mutations, erlotinib-resistant or osimertinib-resistant cell lines were more sensitive to GDH1/RSK2 or CREB inhibitors than EGFR inhibitors, while parental HCC827 and PC9 cells similarly responded to both GDH1/RSK2-CREB and EGFR inhibition (Figure 4B). These data suggest that the combinatorial targeting of GDH1 and RSK2 could be an alternative strategy to attenuate invasive properties in tumors that are EGFR driven and resistant to EGFR inhibitors.

Targeting GDH1/RSK2-CREB attenuates tumor metastasis and promotes T cell activation

We next investigated the therapeutic efficacy of targeting GDH1/RSK2 in blocking tumor metastasis *in vivo* by administering R162 and fmk to A549 and PC9 xenograft mouse models that have WT and mutant forms of EGFR, respectively. The combination effectively decreased tumor progression in both models, but the inhibition of metastatic nodule formation was slightly greater in the PC9 model than the A549 model (Figures 4C, 4D, S6A, and S6B).

In addition to the role of CREB transcription targets in mediating anoikis resistance or invasive potentials, CREB is implicated in immune function.^{13,32} To further investigate the therapeutic efficacy of targeting RSK2/GDH1-CREB signaling in antitumor immunity, we administered R162 and fmk or 666–15 in the 344SQ syngeneic mouse model by engrafting metastatic 344SQ cells through subcutaneous injection.³³ Treatment with either R162/fmk or 666–15 resulted in a dramatic decrease in metastatic tumor nodule formation, with the combination of R162 and fmk showing slightly greater effect than 666–15, while there was no significant change in primary tumor growth (Figures 4E, S6C, and S6D). Therapeutic inhibition of GDH1/RSK2 or CREB resulted in enhanced CD8⁺ T cell infiltration and IFN γ levels in the tumors (Figures 4F and S6E). In addition, increases in activated T cells were observed in plasma collected from mice treated with the combination (Figure 4G). Furthermore, systemic activation of CD8⁺ T cells inversely correlated with the number of metastatic tumor modules in mice treated with the combination (Figure 4H). The dosages of 20 mg/kg of R162 and 25 mg/kg of fmk or 10 mg/kg of 666–15 did not induce significant organ toxicities, which were monitored by assessing organ histology, splenomegaly, and liver and kidney damage (Figures S6F–S6I). Similar results were obtained from another syngeneic mouse model using LLC cells (Figures S6J–S6N). These data suggest that inhibition of RSK2/GDH1-CREB signaling effectively blocks tumor progression and that hindering the immune evasion process may be involved.

EGFR phosphorylates GDH1 at Y135 and contributes to GDH1 activation

To explore the molecular mechanism by which RSK2 and GDH1 are critical in promoting metastasis in EGFR-activated tumors, we investigated the link between EGFR and GDH1/RSK2. MAPK signaling is one of the main pathways involved in mediating the biological responses of EGFR. EGF is known to stimulate RSK2 activation through MEK/ERK pathways and Src-mediated phosphorylation at Y529.³⁴ However, there are no reports on how EGFR signals through GDH1 for cancer progression. To better understand the link between oncogenic tyrosine kinase (OTK) signaling and mitochondrial GDH1, we performed kinase inhibitor profiling by pharmacologically inhibiting multiple OTKs and investigating the effect on GDH activity in four different lung cancer cell lines (Figure 5A). Among 15 inhibitors tested, targeting EGFR commonly attenuated GDH activity. This was further confirmed with a different EGFR inhibitor gefitinib by assessing GDH activity and intracellular α -KG levels (Figure 5B). GDH1 phosphorylation by EGFR enhanced the activity of GDH1 in an *in vitro* coupled activity assay, suggesting that EGFR mediates GDH1 phosphorylation and activates GDH1 (Figure 5C). Furthermore, *in vitro* EGFR kinase assays and subcellular localization assays revealed that EGFR co-localizes with GDH1 in mitochondria and directly phosphorylates GDH1 (Figures 5D–5F).

To determine which tyrosine phosphorylation site in GDH1 contributes to EGFR-mediated phosphorylation and activation, we mutated potential phosphorylation sites that have been identified in human cancers by proteomic profiling (PhosphoSitePlus v.6.6.0.2). These sites include Y135, Y367, Y451, Y464, Y512, Y539, and Y550 in GDH1. Endogenous GDH1 was removed by stable knockdown, and GDH1 variants that are resistant to GDH1 shRNA were expressed. Overexpression of EGFR significantly enhanced GDH1 WT or phosphor-deficient mutants other than Y135F, while activity of Y135F was unaltered by EGFR expression (Figure 5G). Expression of WT active EGFR, but not a kinase dead mutant form of EGFR, D837A, enhanced GDH1 WT activity in cells, and this EGFR effect was abolished in cells expressing GDH1 Y135F (Figure 5H). In line with this observation, Y135F mutation decreased GDH1 activity in cancer cells, whereas the effect was abolished in the presence of EGFR inhibitor erlotinib (Figure 5I). To explore the functional and clinical role of GDH Y135 phosphorylation, a customized phospho-specific antibody against Y135 was generated (Figures S7A and S7B). Through an *in vitro* kinase assay using recombinant active EGFR and purified GDH1 variants as substrates, we found that EGFR directly phosphorylates GDH1 at Y135 (Figure 5J). Furthermore, mutation at Y135 significantly attenuated GDH1 activity, anoikis resistance, and invasive potential in lung cancer cells (Figures 5K and 5L). These data suggest that EGFR directly phosphorylates GDH1 at Y135 and enhances its activity, which consequently promotes cancer cell proliferation, anoikis resistance, and cell invasion.

GDH1 signals through CaMKIV to activate CREB via α -KG

To gain further mechanistic insight into the role of EGFR-mediated GDH1 signaling in CREB activation, we examined whether GDH1 and its product α -KG contribute to CREB activation. We confirmed that the knockdown of GDH1 results in a significant decrease in CREB activation, which was assessed by CREB S133 phosphorylation, as well as anoikis protection in lung cancer cells, whereas the addition of cell permeable α -KG restores the

decreased CREB activation and anoikis resistance, suggesting that GDH1 activates CREB signaling via α -KG (Figures 6A and 6B). We previously demonstrated that GDH1 and α -KG activate CamKK2 in lung cancer cells. CaMKIV is one of the CamKK2 downstream effectors that is known as a potential activator of CREB.³⁵ We found that GDH1 loss results in a significant attenuation in CaMKIV activity, while the replenishment of α -KG fully restores the decreased CaMKIV activity (Figure 6C). Moreover, overexpression of a constitutively active truncated mutant form of CaMKIV, CaMKIV (1–313), rescued the decreased CREB activity and reversed the enhanced anoikis induction in GDH1 knockdown cells (Figures 6D and 6E). These results suggest that GDH1 and α -KG promote CaMKIV activity and consequent CREB phosphorylation, which provides anti-anoikis potential to lung cancer cells.

EGFR-GDH1/RSK2-CREB signaling axes positively correlate in tumor samples from patients with metastatic lung cancer

Our preclinical study demonstrates the crosstalk between RSK2 kinase signaling and the GDH1 metabolic pathway that is mediated by dysregulated EGFR and suggests that targeting these distinct signaling pathways in combination provides a synergistic attenuation of tumor metastasis in lung cancer, including tumors with EGFR-activating and therapy-resistant mutations. To demonstrate the clinical relevance of our finding, we explored the correlations between EGFR, GDH1, RSK2, and CREB activation levels in primary tumor tissues collected from lung cancer patients with different EGFR mutational status (Figure 7A; Table S2). Activation of EGFR, GDH1, RSK2, and CREB was assessed by analyzing immunohistochemistry (IHC) staining of phosphorylated forms of EGFR, GDH1, RSK2, and CREB at Y1068, Y135, S386, and S133, respectively (Figure 7B). The customized phospho-specific antibody against Y135 GDH1 was validated for IHC staining using phospho-Y135 GDH1 blocking peptide in human primary tumor tissues (Figure S7C). Positive correlations were observed between levels of phospho-EGFR, GDH1, or RSK2 and phospho-CREB in both groups of patients with either EGFR mutants or WT. However, the correlations were stronger in tumors collected from patients with EGFR mutations compared with samples from patients with EGFR WT (Figure 7C). Significant correlations between activation of EGFR, GDH1, RSK2, and CREB were found in a larger cohort of tumor samples obtained from patients with metastatic lung cancer (Figures 7D and 7E). We further demonstrated that the correlation between p-GDH1 and p-CREB that are linked through CamKK2-CaMKIV, as shown in Figure 6, would be most prominent when cells are lacking LKB1 that often serves as an alternative kinase of CamKK2 (Figures S7D and S7E). These data clinically validate the functional relationship between EGFR, GDH1/RSK2, and CREB in human lung cancer.

DISCUSSION

Understanding the molecular mechanisms mediating drug synergy in combination therapies facilitates further optimization of valuable drug interactions and can provide significant insights into the underlying biology. Our study delineates the mechanism of action of a unique combination cancer therapy by confirming a signaling crosstalk in which oncogenic driver EGFR-activated cellular kinase pathway and metabolic factors are

intertwined to promote tumor metastasis. We identified that the RSK2 and GDH1 compensatory signaling axes coordinately program the acquisition of anoikis resistance and pro-invasive, pro-migratory, and pro-metastatic signaling through activation of CREB-mediated transcription. The effect of dual targeting was evident in lung cancer cells with EGFR-activating and inhibitor-resistance mutations as the EGFR-mediated activation of GDH1 by phosphorylation at tyrosine 135 and RSK2 via the MAPK pathway. While RSK2 directly activates CREB by phosphorylation at serine 133, GDH1 contributes to CREB activation by α -KG signaling through CaMKIV (Figure 7F).

Restoration of CREB activation by CREB phospho-mimetic mutant S133D expression significantly, but not fully, rescued the decreased invasion and anoikis resistance in cancer cells resulting from target downregulation of both GDH1 and RSK2. This implies that CREB is a predominant, albeit not the sole, contributor that confers GDH1- and RSK2-mediated pro-invasive and anti-anoikis potentials. There may exist alternative downstream effectors that signal through GDH1 and RSK2 to promote tumor metastasis. These effectors could be cellular signaling components other than the factors involved in the AKT, MAPK, TGF- β , JAK/STAT, and NF- κ B pathways we examined or metabolic pathways other than glutaminolysis. For instance, these two signaling axes may manage metabolic factors not directly connected to glutamine metabolism, such as glycolysis or the urea cycle. A recent study reports that RSK phosphorylates 6-phosphofructo-2-kinase/fructose-2,6-bisphosphatase 2 (PFKFB2), an enzyme in the glycolysis pathway, and targeting RSK attenuates PFKFB2 activity and the flux of glycolysis in melanoma cells harboring BRAF mutation.³⁶ It is plausible that in addition to impairment of the CREB transcription pathway, simultaneous target downregulation of GDH1 and RSK2 may inhibit both glutaminolysis and glycolysis through GDH1 and RSK2, respectively, leading to further attenuation of tumor progression. A global metabolite profiling of cells treated with the combination may further reveal other metabolic pathways that contribute to the synergistic effect.

Targeting RSK/GDH or CREB resulted in increased CD8 T cell infiltration (TIL) in tumors, indicating enhanced immune surveillance in cancer. CREB governs gene expression of many signaling effectors involved in tumor progression and immune regulation.³² Interestingly, treatment with the RSK/GDH inhibitors combination, but not with the CREB inhibitor, induced systemic activation of CD8 T cells. These findings suggest that the combinatorial treatment may enhance immunosurveillance, but the mechanism of enhanced TIL and activation of CD8 T cells in the circulating system may differ. TIL may involve CREB transcriptional activation, whereas systemic T cell activation induced by the combination could be independent of CREB signaling. Detailed immune-oncology studies are warranted to better understand how these signaling axes contribute to antitumor immunity.

Combination therapies have become a common area of investigation in the development of therapeutic strategies for cancer treatment. Very few studies report effective combinatorial anticancer strategies that target both cellular kinase signaling and a metabolic pathway. Trastuzumab, a monoclonal antibody against HER2, when combined with glycolysis inhibition using 2-deoxyglucose (2-DG) shows synergistic inhibition of breast cancer cell growth.³⁷ Understanding the biological mechanism of drug combinations will likely enable us to better optimize combined treatments and to benefit from drug synergies. In this study,

we provide evidence that targeting cellular and metabolic signaling effectors, RSK2 and GDH1, using their specific inhibitors synergistically attenuated pro-metastasis potential in lung cancer. We found that the effect of the combination on mitigating invasion is more evident in cancer cells with EGFR-activating and inhibitor-resistant mutations compared with cells with WT EGFR. EGFR-induced phosphorylation and activation of GDH1 and RSK2 as downstream effectors may explain the different effect.

The activation of RSK2/GDH1 signaling positively correlates with the status of EGFR activation, which is often mediated by mutations. Overexpression of EGFR, not necessarily mutation, can also result in enhanced EGFR activation. Our study provides a rationale for targeted combination therapy with activity in both EGFR mutant and WT NSCLC. NSCLC patients who would benefit more from the combination will be individuals with activated EGFR including the group harboring activating mutations such as exon 19 deletion or L858R mutation, which constitute approximately 31% of NSCLC patients.³⁸

Resistance to EGFR inhibitors in EGFR-mutated tumors has been a major challenge. While EGFR inhibitors have benefited many lung cancer patients with activating mutations, almost all eventually acquire resistance.³⁹ In our study, EGFR inhibitor-resistant cells that were not responsive to erlotinib or osimertinib treatment responded to the pharmacological inhibition of GDH1 and RSK2. Thus, our study may make an impactful fundamental contribution to improve cancer treatment in patients diagnosed with advanced metastatic cancers with activated EGFR who often acquire EGFR therapy resistance and currently lack effective treatment options.

Limitations of the study

While our phosphorylation pathway profiling array detecting 55 phosphorylations in five signaling pathways revealed CREB as one of the pivotal GDH1 and RSK2 signal converging factors, we have not globally searched whether any of the other unknown phosphorylated factors are mediating the synergistic effect. A future investigation of these unknown factors through mass spectrometry-based phospho-proteomics and metabolomics approaches is warranted. In addition, while we have shown that tumors harboring EGFR mutations are more susceptible to dual inhibition of GDH1 and RSK2 than EGFR WT tumors, it remains unknown how each of the distinct mutations in EGFR leads to GDH1/RSK2-CREB activation in cancer cells and altered therapeutic response in patients. Detailed mutational approaches, pharmacokinetics studies, and clinical trials are warranted to further evaluate and optimize the treatment options for the proposed combination therapy.

STAR★METHODS

RESOURCE AVAILABILITY

Lead contact—Further information and resources and reagents requests should be asked and will be fulfilled by the lead contact, Sumin Kang (smkang@emory.edu).

Materials availability—All reagents generated during this study are available from the lead contact.

Data and code availability

- All data reported in this paper will be shared by the lead contact upon request.
- This paper does not report original code.
- Any additional information required to reanalyze the data reported in this paper is available from the lead contact upon request.

EXPERIMENTAL MODEL AND SUBJECT DETAILS

***In vivo* animal studies**—Animal experiments were conducted according to protocols approved by the Emory University’s Institutional Animal Care and Use Committee (IACUC). Athymic nude, C57BL/6J, and 129/Sv mice (female, 4-week-old, Envigo and Jackson Laboratory) were used for animal experiments.

Human tumor sample studies—Approval to use human specimens was given by the Emory University’s Institutional Review Board (IRB). All clinical samples from lung cancer patients were collected with informed consent under Health Insurance Portability and Accountability Act approved protocols. Formalin fixed paraffin embedded tumors from lung cancer patient were obtained from US Biomax. Clinical information related to the subjects can be found at Table S2.

Human and murine cell line culture—Human lung cancer cell lines including A549, H157, PC9, and HCC827 and murine lung cancer cell line 344SQ were cultured in RPMI 1640 medium with 10% fetal bovine serum (FBS). 293T, MRC-5, and LLC cells were cultured in Dulbecco’s modified Eagle’s medium (DMEM) and BEAS-2B in DMEM/F12 with 10% FBS. Cell line authentication was carried out using STR profiling.

METHOD DETAILS

Metabolic inhibitor and kinase inhibitor screens—To screen for effective metabolic inhibitors that attenuate invasion and anoikis resistance in combination with fmk treatment, A549 cells were treated with mitomycin C for 2 h and treated with cancer-related metabolic enzyme inhibitors at sublethal doses (Polydatin, 20 μ M; A922500, 45 μ M; ADI, 200 μ M; R162, 20 μ M; Lometrexol, 10 μ M; 3PO, 10 μ M; Triparanol, 1 μ M; Methotrexate, 1 μ M; Brequinar, 20 μ M; Clorgyline, 1 μ M; ME1, 20 μ M; BSO, 400 μ M; RO48-8071, 10 μ M; DAHP, 0.5 mM) and fmk (5 μ M) followed by invasion assay and anoikis assay. For profiling of kinase inhibitors’ effects on GDH activity in cells, cells were treated with 10 μ M drugs for 4 h and GDH activity assessed using cell lysates.

Establishment of stable or drug resistant cell lines—Lentivirus production and infection for RSK2, GDH1, or CREB knockdown in human cancer cell lines were performed as previously described.³⁰ Cells were transduced with retroviral vectors harboring GDH1 WT or Y135F followed by 300 mg/mL hygromycin selection for stable expression, and GFP-luciferase genes for bioluminescent imaging. HCC827 and PC9 erlotinib or osimertinibresistant cell lines were generated by culturing parental cells with escalating doses of erlotinib or osimertinib. The resistant cell lines were maintained in 1 μ M of

erlotinib or osimertinib, which were removed from the media for 1 day before conducting experiments.

Cell invasion, migration, and anoikis assays—For cell invasion or migration assays, approximately 5×10^4 cells were pretreated with mitomycin C (10 $\mu\text{g}/\text{mL}$) for 2 h prior to seeding on 8 μm pore sized transwell inserts in serum-free media. For PDX tumors, single cell suspended 5×10^5 cells were used for invasion assay. The chambers were coated with Matrigel (272 $\mu\text{g}/\text{mL}$) for the cell invasion assay. Media containing 10% FBS was added to the lower chambers and incubated for 16 h. The invaded or migrated cells on the bottom of the chambers were stained with 0.5% crystal violet, counted, and normalized to the proliferation rate assessed by parallel CellTiter-Glo cell viability assay. For anoikis assay, approximately 5×10^5 cells/well were seeded on 1% agarose-coated 6-well plates for 48 h. Cells were collected and detachment-induced apoptotic cell death was assessed by FITC Annexin V apoptosis detection kit and flow cytometry analysis according to the manufacturer's instruction.

GDH activity assays—GDH activity assay was performed as previously described.^{30,42} Briefly, 20 μg of cell lysates was added to the reaction buffer containing 100 mM ammonium acetate, 50 mM triethanolamine, 2.6 mM EDTA, 100 μM NADPH, and 8 mM α -KG. The NADPH oxidation was observed at 340 nm.

In vitro kinase assays—Purified GDH1 from bovine liver (0.35 μg ; Sigma Aldrich G2626) or GDH1 with or without the Y135F mutation enriched from 2×10^6 of 293T cells was incubated with recombinant active EGFR T790M/L858R (0.2 μg ; Invitrogen PV4879) in assay buffer (50 mM HEPES pH 7.5, 0.01% Triton X-100, 10 mM MgCl_2 , 1 mM EGTA, and 200 μM ATP) at a final volume of 40 μL for 30 min at 30°C. The phosphorylation of GDH1 by EGFR was determined by either pan-pY99 or phospho-GDH1(Y135) Western blot. For CaMKIV kinase activity assay, endogenous CaMKIV was immunoprecipitated with anti-CaMKIV antibody and subjected to a kinase assay using a reaction buffer containing 40 mM Tris [pH 7.5], 20 mM MgCl_2 , 40 μM ATP, 50 μM DTT, 1 $\mu\text{g}/\text{mL}$ calmodulin, 400 μM CaCl_2 , 0.1 mg/mL BSA, and 200 $\mu\text{g}/\text{mL}$ of CaMKIV synthetic substrate peptides. The activity of CaMKIV was determined by ADP-Glo Kinase Assay (Promega V6930).

Metabolic assays—Ammonia production and glutamine consumption levels were determined using Ammonia Assay Kit (Abcam) and Glutamine/Glutamate-Glo assay (Promega), respectively. Intracellular ROS levels were quantified using CM-H₂DCFDA (Invitrogen). Intracellular ATP concentrations were measured by ATP bioluminescent somatic cell assay kit (Sigma-Aldrich). Intracellular α -KG levels were determined using alpha-KG Assay Kit (Abcam). Briefly, 2×10^6 cells were collected for each group and cell volume was estimated by comparing the size of the cell pellet with the size of the known volume of PBS. Cell pellets were homogenized and centrifuged. The supernatant was further deproteinized using Amicon 10k centrifugal filter (Millipore) and applied to alpha-KG measurement.

CREB DNA binding assay—CREB DNA binding activity was determined using CREB (Phospho-Ser133) Transcription Factor Assay Kit (Cayman Chemical). In brief, 10 µg of nuclear extracts were collected using NE-PER Nuclear and Cytoplasmic Extraction Reagents (Thermo Scientific) and incubated in a 96-well plate pre-coated with cAMP response element (CRE). The activated CREB-CRE complex was captured with phospho-Ser133 CREB antibody and quantified by ELISA.

Quantitative RT-PCR—1 µg of total RNA isolated from cells was converted to cDNA using High-Capacity cDNA Reverse Transcription Kit (Applied Biosystems). Quantitative PCR was performed using iTaq Universal SYBR Green Supermix (Bio-Rad). Relative gene expression was evaluated by comparative CT method and normalized using GAPDH. The following primers were used for amplification. PTK6: forward 5'-TGTGGAGTGTCTGCGTCCAATACA-3' and reverse 5'-AGGCCAAGCTCTCAAGACACAAGA-3', ING3: forward 5'-CAGCCTCTTC TAACAATGCCTA-3' and reverse 5'-CTTCATCAAACAAAAGGACCAC-3', Fascin-1: forward 5'-AGGCGGCCAACGAGAGGAAC-3' and reverse 5'-ACGATGATGGGGCGGTTGAT-3', GAPDH: forward 5'-GACATCAAGAAGGTGGTGAA-3' and reverse 5'-TGTCATAC CAGG AAATGAGC-3'.

Subcellular localization analysis—Mitochondrial and cytosolic fractions were obtained using Mitochondria Isolation Kit (89874, Thermo Fisher) following the manufacturer's instructions. In brief, 2×10^7 cells were pelleted and 800 µL of Reagent A, 10 µL of Reagent B, and 800 µL of Reagent C were sequentially added on ice and the mixture was centrifuged at $700 \times g$ for 10 min at 4°C. The supernatant was used as the cytosol fraction and the pellet was used as the mitochondrial fraction after washing with 500 µL of Reagent C and dissolving in 50 µL of PBS containing the protease inhibitors. The mitochondrial and cytosolic fractions were analyzed by Western blot assays. COX IV and β-actin were used as markers for the mitochondrial and the cytosolic fractions, respectively.

Immunofluorescence microscopy—Cells cultured on the glass coverslip were treated with 100 nM of MitoTracker Red CMXros (Invitrogen) for 30 min at 37°C. Cells were then fixed and permeabilized with PHEMO buffer (68 mM PIPES, 25 mM HEPES, 15 mM EGTA, 3 mM MgCl₂, 0.05% glutaraldehyde, 3.7% formaldehyde, 0.5% Triton X-100) for 10 min. Cells were incubated with PBS containing 10% goat serum and stained with primary antibody specific for GDH1 or EGFR at a dilution of 1:100 and anti-rabbit IgG Alexa Fluor 488 at a dilution of 1:1000 in PBS containing 5% goat serum for an hour each. Cells were mounted with antifade mounting solution with DAPI and imaged using Leica SP8 confocal microscope.

In vivo mouse model studies—Animal experiments were performed according to the protocol approved by the Institutional Animal Care and Use Committee of Emory University. Nude mice (athymic nu/nu, female, 4-week old, Envigo) were intravenously injected with 1×10^6 cells of A549-luc-GFP or PC9-luc-GFP. From the next day following xenograft injection, mice were intraperitoneally injected with vehicle, R162 (20 mg/kg/day) and/or fmk (25 mg/kg) 3 times/week. Mice were intraperitoneally administered 75

mg/kg of D-luciferin (Perkin Elmer) and bioluminescent images were obtained once a week using IVIS Spectrum *in vivo* imaging system (Perkin Elmer). For syngeneic mouse models, 344SQ 129/Sv or LLC C57BL/6J mice (female, 4-week old, Envigo and Jackson Laboratory) were subcutaneously or intravenously injected with 1×10^6 of 344SQ cells or 2×10^6 of LLC cells, respectively. When tumor size reached 100 mm^3 at 7 days (344SQ) or 5 days (LLC) after injection, mice were administered 20 mg/kg of R162 and 25 mg/kg of fmk in combination 3 times/week or 10 mg/kg of 666–15 once a week *via* intraperitoneal injection for 29 or 41 days, respectively. The tumor nodules in lungs were hematoxylin and eosin (H&E) stained and tumor infiltrated CD8 T cells and IFN γ levels were monitored by IHC staining. Images were scanned and numbers of tumor nodules and CD8 T cells were analyzed by ImageJ software. Drug organ toxicities including splenomegaly, liver damage, and kidney injury were monitored by histological staining, Mouse ALT assay, and Mouse Kidney Toxicity Multiplex Assay according to the manufacturers' instructions.

T cell activation study—CD8 T cells in lung tumors were assessed by immunohistochemistry staining. CD8-positive T cells were counted in 3 randomly obtained areas from each lung section. Activation of T cells were measured by analyzing CD3- and CD69-positive population in mice plasma by flow cytometry.

Immunohistochemistry staining—Approval to use human specimens was given by the Institutional Review Board (IRB) of Emory University. All clinical samples were collected with informed consent under approved protocols from Health Insurance Portability and Accountability Act (HIPAA). Formalin-fixed, paraffin-embedded tissues with EGFR variants from lung cancer patients were obtained from the Cancer Tissue and Pathology Shared Resource of Winship Cancer Institute. Clinical information including EGFR mutation status for the patients was obtained from the files at Emory University Hospital with approval and under the guidelines of the Emory IRB. Primary tumors and matched lymph node metastasized tumors from lung cancer patients were obtained from US Biomax (TMA LC817b). Sectioned human and mouse tumor tissues were deparaffinized, rehydrated, and incubated in methanol containing 3% hydrogen peroxide for endogenous peroxidase activity suppression. Antigen retrieval was performed using 10 mM sodium citrate (pH 6.0). The primary antibodies were applied to the tissues at dilutions of 1:100 (anti-p-EGFR Y1068, p-GDH Y135, p-CREB S133, LKB1, CD8, and IFN γ antibodies) and 1:200 (anti-p-RSK S380 antibody) overnight. The tissues were then stained with 3,3'-diaminobenzidine and hematoxylin. The stained tissues were scored as 0 for no staining, +1, +2, and +3 for weak, moderate, and strong staining, respectively. Staining scores were multiplied by the ratio of tumor area stained for p-EGFR, p-RSK, and p-GDH staining of non-tissue microarray specimens.

QUANTIFICATION AND STATISTICAL ANALYSIS

Graphical presentation and statistical analysis were performed using GraphPad Prism 9.0. Statistical analysis of significance was based on unpaired two-tailed Student's *t* test for Figures 1A, 3A–3C, 4C, 4D, 5G, S6A, and S6B, Pearson's *r* for Figures 4H, 7C, and S6M, chi-square test for Figures 7D and S7E, and one-way ANOVA for all other figures. Data with error bars represent mean \pm standard deviation (SD), except for Figures 1E, S1H,

and S5A–S5D, which indicates mean \pm standard error of the mean (SEM). The number of experimental replicates is listed in each figure panel. Statistical analyses were performed based on the homogeneity of variances and assumptions of normal distribution. *p* values of less than 0.05 were considered statistically significant.

Supplementary Material

Refer to Web version on PubMed Central for supplementary material.

ACKNOWLEDGMENTS

We acknowledge Dr. Anthea Hammond for editorial assistance. This work was supported in part by NIH grants R01 CA175316 (S.K.), R01 CA207768 (S.K.), R01 CA266613 (S.K.), R37 CA249305 (L.J.), R01 CA269782 (L.J.), F99 CA264407 (A.C.B.), P50 CA217691 (S.R. and H.F.), and P01 CA257906 (H.F. and S.R.); DoD W81XWH-21-1-0213 (S.K.); and the Integrated Cellular Imaging resource of Winship Cancer Institute of Emory University under NIH/NCI P30 CA138292. A.C.B. is an NIH pre-doctoral fellow. S.K. is an American Cancer Society Basic Research Scholar and Georgia Cancer Coalition Scholar.

REFERENCES

- Gupta GP, and Massagué J (2006). Cancer metastasis: building a framework. *Cell* 127, 679–695. 10.1016/j.cell.2006.11.001. [PubMed: 17110329]
- Brognaud J, and Hunter T (2011). Protein kinase signaling networks in cancer. *Curr. Opin. Genet. Dev.* 21, 4–11. 10.1016/j.gde.2010.10.012. [PubMed: 21123047]
- Gerber DE (2008). EGFR inhibition in the treatment of non-small cell lung cancer. *Drug Dev. Res.* 69, 359–372. 10.1002/ddr.20268. [PubMed: 19562083]
- Khalil MY, Grandis JR, and Shin DM (2003). Targeting epidermal growth factor receptor: novel therapeutics in the management of cancer. *Expert Rev. Anticancer Ther.* 3, 367–380. 10.1586/14737140.3.3.367. [PubMed: 12820779]
- Mok TS, Wu YL, Thongprasert S, Yang CH, Chu DT, Saijo N, Sunpaweravong P, Han B, Margono B, Ichinose Y, et al. (2009). Gefitinib or carboplatin-paclitaxel in pulmonary adenocarcinoma. *N. Engl. J. Med.* 361, 947–957. 10.1056/NEJMoa0810699. [PubMed: 19692680]
- Passaro A, Jänne PA, Mok T, and Peters S (2021). Overcoming therapy resistance in EGFR-mutant lung cancer. *Nat. Cancer* 2, 377–391. 10.1038/s43018-021-00195-8. [PubMed: 35122001]
- Wee P, and Wang Z (2017). Epidermal growth factor receptor cell proliferation signaling pathways. *Cancers* 9, 52. 10.3390/cancers9050052. [PubMed: 28513565]
- Dehan E, Bassermann F, Guardavaccaro D, Vasiliver-Shamis G, Cohen M, Lowes KN, Dustin M, Huang DCS, Taunton J, and Pagano M (2009). betaTrCP- and Rsk1/2-mediated degradation of BimEL inhibits apoptosis. *Mol. Cell* 33, 109–116. 10.1016/j.molcel.2008.12.020. [PubMed: 19150432]
- Frisch SM (2000). Anoikis. *Methods Enzymol.* 322, 472–479. 10.1016/s0076-6879(00)22043-0. [PubMed: 10914040]
- Simpson CD, Anyiwe K, and Schimmer AD (2008). Anoikis resistance and tumor metastasis. *Cancer Lett.* 272, 177–185. 10.1016/j.canlet.2008.05.029. [PubMed: 18579285]
- Frisch SM, and Screaton RA (2001). Anoikis mechanisms. *Curr. Opin. Cell Biol.* 13, 555–562. 10.1016/s0955-0674(00)00251-9. [PubMed: 11544023]
- Jin L, Li D, Lee JS, Elf S, Alesi GN, Fan J, Kang HB, Wang D, Fu H, Taunton J, et al. (2013). p90 RSK2 mediates antianoikis signals by both transcription-dependent and -independent mechanisms. *Mol. Cell Biol.* 33, 2574–2585. 10.1128/MCB.01677-12. [PubMed: 23608533]
- Wen AY, Sakamoto KM, and Miller LS (2010). The role of the transcription factor CREB in immune function. *J. Immunol.* 185, 6413–6419. 10.4049/jimmunol.1001829. [PubMed: 21084670]

14. Cohen MS, Zhang C, Shokat KM, and Taunton J (2005). Structural bioinformatics-based design of selective, irreversible kinase inhibitors. *Science* 308, 1318–1321. 10.1126/science.1108367. [PubMed: 15919995]
15. Li BX, Gardner R, Xue C, Qian DZ, Xie F, Thomas G, Kazmierczak SC, Habecker BA, and Xiao X (2016). Systemic inhibition of CREB is well-tolerated in vivo. *Sci. Rep.* 6, 34513. 10.1038/srep34513. [PubMed: 27694829]
16. Hsu PP, and Sabatini DM (2008). Cancer cell metabolism: warburg and beyond. *Cell* 134, 703–707. 10.1016/j.cell.2008.08.021. [PubMed: 18775299]
17. Warburg O (1956). On the origin of cancer cells. *Science* 123, 309–314. 10.1126/science.123.3191.309. [PubMed: 13298683]
18. Kim JW, and Dang CV (2006). Cancer's molecular sweet tooth and the Warburg effect. *Cancer Res.* 66, 8927–8930. 10.1158/0008-5472.CAN-06-1501. [PubMed: 16982728]
19. Frezza C, and Gottlieb E (2009). Mitochondria in cancer: not just innocent bystanders. *Semin. Cancer Biol.* 19, 4–11. 10.1016/j.semcancer.2008.11.008. [PubMed: 19101633]
20. DeBerardinis RJ, and Chandel NS (2016). Fundamentals of cancer metabolism. *Sci. Adv.* 2, e1600200. 10.1126/sciadv.1600200. [PubMed: 27386546]
21. Hanahan D, and Weinberg RA (2011). Hallmarks of cancer: the next generation. *Cell* 144, 646–674. 10.1016/j.cell.2011.02.013. [PubMed: 21376230]
22. Moreadith RW, and Lehninger AL (1984). The pathways of glutamate and glutamine oxidation by tumor cell mitochondria. Role of mitochondrial NAD(P)⁺-dependent malic enzyme. *J. Biol. Chem.* 259, 6215–6221. [PubMed: 6144677]
23. Wise DR, and Thompson CB (2010). Glutamine addiction: a new therapeutic target in cancer. *Trends Biochem. Sci.* 35, 427–433. 10.1016/j.tibs.2010.05.003. [PubMed: 20570523]
24. Wang JB, Erickson JW, Fuji R, Ramachandran S, Gao P, Dinavahi R, Wilson KF, Ambrosio ALB, Dias SMG, Dang CV, and Cerione RA (2010). Targeting mitochondrial glutaminase activity inhibits oncogenic transformation. *Cancer Cell* 18, 207–219. 10.1016/j.ccr.2010.08.009. [PubMed: 20832749]
25. Robinson MM, McBryant SJ, Tsukamoto T, Rojas C, Ferraris DV, Hamilton SK, Hansen JC, and Curthoys NP (2007). Novel mechanism of inhibition of rat kidney-type glutaminase by bis-2-(5-phenylacetamido-1, 2, 4-thiadiazol-2-yl)ethyl sulfide (BPTES). *Biochem. J.* 406, 407–414. 10.1042/BJ20070039. [PubMed: 17581113]
26. Seltzer MJ, Bennett BD, Joshi AD, Gao P, Thomas AG, Ferraris DV, Tsukamoto T, Rojas CJ, Slusher BS, Rabinowitz JD, et al. (2010). Inhibition of glutaminase preferentially slows growth of glioma cells with mutant IDH1. *Cancer Res.* 70, 8981–8987. 10.1158/0008-5472.CAN-10-1666. [PubMed: 21045145]
27. Jin L, Chun J, Pan C, Kumar A, Zhang G, Ha Y, Li D, Alesi GN, Kang Y, Zhou L, et al. (2018). The PLAG1-GDH1 Axis promotes anoikis resistance and tumor metastasis through CamKK2-AMPK signaling in LKB1-deficient lung cancer. *Mol. Cell* 69, 87–99.e7. 10.1016/j.molcel.2017.11.025. [PubMed: 29249655]
28. Farris JC, Pifer PM, Zheng L, Gottlieb E, Denvir J, and Frisch SM (2016). Grainyhead-like 2 reverses the metabolic changes induced by the oncogenic epithelial-mesenchymal transition: effects on anoikis. *Mol. Cancer Res.* 14, 528–538. 10.1158/1541-7786.MCR-16-0050. [PubMed: 27084311]
29. Pifer PM, Farris JC, Thomas AL, Stoilov P, Denvir J, Smith DM, and Frisch SM (2016). Grainyhead-like 2 inhibits the coactivator p300, suppressing tubulogenesis and the epithelial-mesenchymal transition. *Mol. Biol. Cell* 27, 2479–2492. 10.1091/mbc.E16-04-0249. [PubMed: 27251061]
30. Jin L, Li D, Alesi GN, Fan J, Kang HB, Lu Z, Boggon TJ, Jin P, Yi H, Wright ER, et al. (2015). Glutamate dehydrogenase 1 signals through antioxidant glutathione peroxidase 1 to regulate redox homeostasis and tumor growth. *Cancer Cell* 27, 257–270. 10.1016/j.ccell.2014.12.006. [PubMed: 25670081]
31. Ghandi M, Huang FW, Jané-Valbuena J, Kryukov GV, Lo CC, McDonald ER 3rd, Barretina J, Gelfand ET, Bielski CM, Li H, et al. (2019). Next-generation characterization of the cancer cell line encyclopedia. *Nature* 569, 503–508. 10.1038/s41586-019-1186-3. [PubMed: 31068700]

32. Gu C, Wang L, Zurawski S, and Oh S (2019). Signaling cascade through DC-ASGPR induces transcriptionally active CREB for IL-10 induction and immune regulation. *J. Immunol.* 203, 389–399. 10.4049/jimmunol.1900289. [PubMed: 31175164]
33. Gibbons DL, Lin W, Creighton CJ, Rizvi ZH, Gregory PA, Goodall GJ, Thilaganathan N, Du L, Zhang Y, Pertsemlidis A, and Kurie JM (2009). Contextual extracellular cues promote tumor cell EMT and metastasis by regulating miR-200 family expression. *Genes Dev.* 23, 2140–2151. 10.1101/gad.1820209. [PubMed: 19759262]
34. Kang S, Dong S, Guo A, Ruan H, Lonial S, Khoury HJ, Gu TL, and Chen J (2008). Epidermal growth factor stimulates RSK2 activation through activation of the MEK/ERK pathway and src-dependent tyrosine phosphorylation of RSK2 at Tyr-529. *J. Biol. Chem.* 283, 4652–4657. 10.1074/jbc.M709673200. [PubMed: 18156174]
35. Sun P, Enslin H, Myung PS, and Maurer RA (1994). Differential activation of CREB by Ca²⁺/calmodulin-dependent protein kinases type II and type IV involves phosphorylation of a site that negatively regulates activity. *Genes Dev.* 8, 2527–2539. 10.1101/gad.8.21.2527. [PubMed: 7958915]
36. Houles T, Gravel SP, Lavoie G, Shin S, Savall M, Méant A, Grondin B, Gaboury L, Yoon SO, St-Pierre J, and Roux PP (2018). RSK regulates PFK-2 activity to promote metabolic rewiring in melanoma. *Cancer Res.* 78, 2191–2204. 10.1158/0008-5472.CAN-17-2215. [PubMed: 29440170]
37. Zhao Y, Liu H, Liu Z, Ding Y, Ledoux SP, Wilson GL, Voellmy R, Lin Y, Lin W, Nahta R, et al. (2011). Overcoming trastuzumab resistance in breast cancer by targeting dysregulated glucose metabolism. *Cancer Res.* 71, 4585–4597. 10.1158/0008-5472.CAN-11-0127. [PubMed: 21498634]
38. Kumari N, Singh S, Haloi D, Mishra SK, Krishnani N, Nath A, and Neyaz Z (2019). Epidermal growth factor receptor mutation frequency in squamous cell carcinoma and its diagnostic performance in cytological samples: a molecular and immunohistochemical study. *World J. Oncol.* 10, 142–150. 10.14740/wjon1204. [PubMed: 31312281]
39. Stewart EL, Tan SZ, Liu G, and Tsao MS (2015). Known and putative mechanisms of resistance to EGFR targeted therapies in NSCLC patients with EGFR mutations—a review. *Transl. Lung Cancer Res.* 4, 67–81. 10.3978/j.issn.2218-6751.2014.11.06. [PubMed: 25806347]
40. Wilson AA, Murphy GJ, Hamakawa H, Kwok LW, Srinivasan S, Hovav AH, Mulligan RC, Amar S, Suki B, and Kotton DN (2010). Amelioration of emphysema in mice through lentiviral transduction of long-lived pulmonary alveolar macrophages. *J. Clin. Invest.* 120, 379–389. 10.1172/JCI36666. [PubMed: 20038801]
41. Greulich H, Chen TH, Feng W, Jänne PA, Alvarez JV, Zappaterra M, Bulmer SE, Frank DA, Hahn WC, Sellers WR, and Meyerson M (2005). Oncogenic transformation by inhibitor-sensitive and -resistant EGFR mutants. *PLoS Med.* 2, e313. 10.1371/journal.pmed.0020313. [PubMed: 16187797]
42. Zaganas I, Spanaki C, Karpusas M, and Plaitakis A (2002). Substitution of Ser for Arg-443 in the regulatory domain of human housekeeping (GLUD1) glutamate dehydrogenase virtually abolishes basal activity and markedly alters the activation of the enzyme by ADP and L-leucine. *J. Biol. Chem.* 277, 46552–46558. 10.1074/jbc.M208596200. [PubMed: 12324473]

Highlights

- Dual targeting of RSK2 and GDH1 synergistically attenuates cancer metastasis
- RSK2 and GDH1 coordinatively enhance the CREB activity
- EGFR phosphorylates GDH1 at Y135 and activates GDH1
- The activities of EGFR, GDH1, RSK2, and CREB correlate in primary patient tumors

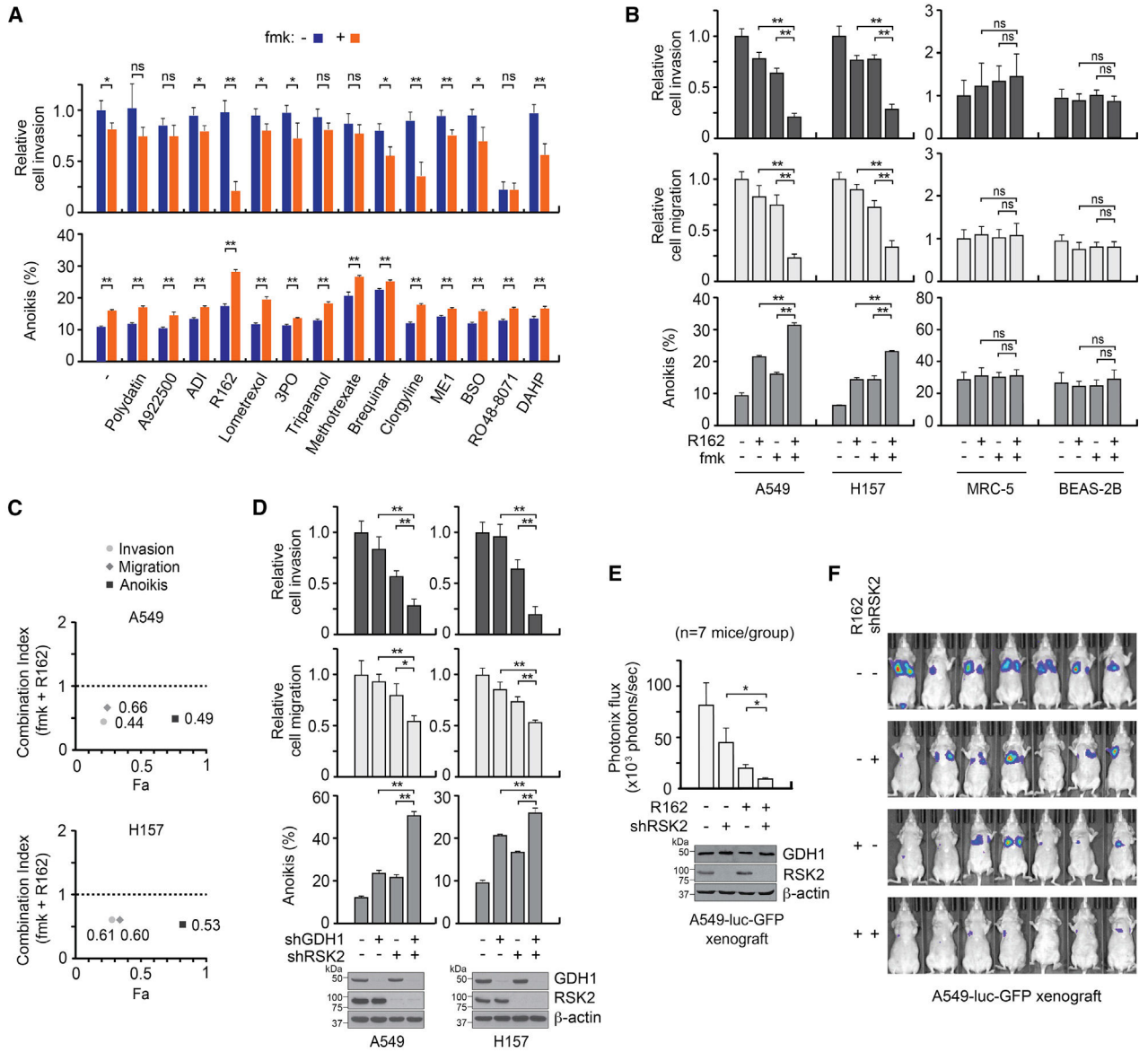


Figure 1. Metabolic inhibitor profiling identifies GDH1 and RSK2 as a synthetic target combination to attenuate invasive and metastatic potentials in lung cancer

(A) Cancer-related metabolic inhibitors and RSK inhibitor treatment effect on cancer cell invasion and anoikis induction. Cell invasion assay (top) and anoikis assay (bottom) of A549 cells treated with fmk and inhibitors targeting cancer-inducing metabolic enzymes. Cells were pretreated with mitomycin C (10 μ g/mL) for 2 h followed by fmk (5 μ M) and/or metabolic inhibitor treatment at concentrations indicated in STAR Methods in Matrigel-coated transwell chambers for 24 h to assess invasive potential. Cells were seeded on 1% agarose-treated plates and treated with the inhibitors for 48 h, and detachment-induced cell death was assessed by annexin V staining.

(B) Effect of R162 and fmk on cell invasion, migration, and anoikis induction. Lung cancer cells (A549 and H157) and non-cancerous cells (MRC-5 and BEAS-2B) were seeded into

transwell chambers that are Matrigel coated (top) or uncoated (middle), or 1% agarose-treated plates (bottom), followed by R162 (20 μ M) and/or fmk (5 μ M) treatment.

(C) Fa-combination index plots describing the R162 and fmk drug effect on invasion, migration, and anoikis induction. CI values (CI < 1: synergism) were obtained by CompuSyn.

(D) Effect of genetic inhibition of GDH1 and RSK2 on invasion, migration, and anoikis induction. A549 and H157 cells with stable knockdown of GDH1 and RSK2 were applied to invasion, migration, and anoikis assays as described in (A) and (B). The knockdown efficacy was assessed by immunoblotting.

(E and F) Effect of RSK2 and GDH1 inhibition on tumor progression in vivo. A549-luc-GFP cells with or without RSK2 knockdown were injected into the tail veins of mice, and 20 mg/kg of R162 was intraperitoneally administered. Average photonic flux (E) and bioluminescent images (F) of each group at week 7 are shown. RSK2 and GDH1 expression in cells used for xenograft injection is shown. Data represent mean \pm SEM from seven mice for each group for (E) and mean \pm SD from three replicates for (A)–(D). p values were determined by two-tailed Student's t test for (A) and one-way ANOVA for the others (ns, not significant; *0.01 < p < 0.05; **p < 0.01). See also Table S1 and Figure S1.

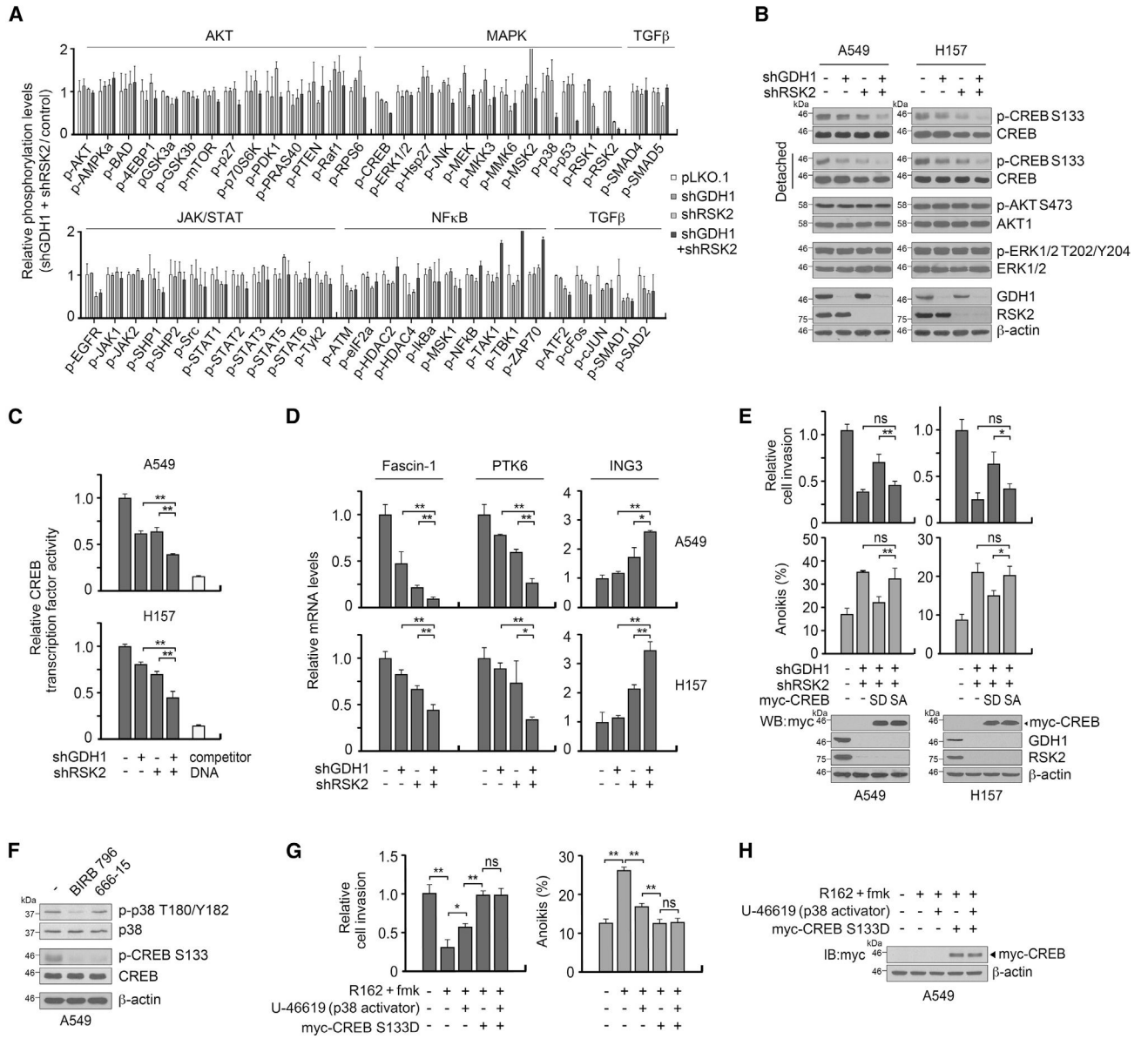


Figure 2. RSK2 and GDH1 cooperatively confer invasive and anoikis resistant potentials through CREB activation

(A) Phosphorylation levels altered by GDH1 and RSK2 knockdown. Human phosphorylation pathway profiling array results were obtained using 55 antibodies detecting AKT, JAK/STAT, MAPK, NF-κB, and TGF-β signaling in A549 lysates.

(B) A549 and H157 cells with GDH1 and RSK2 knockdown were cultured under attached or detached conditions and assayed for CREB, AKT, and ERK1/2 phosphorylation by immunoblotting. GDH1, RSK2, and β-actin blots were obtained from attached conditions, and similar stable knockdown efficacy was observed in detached conditions.

(C) Effect of RSK2 and GDH1 knockdown on CREB activity was assessed by CREB transcription factor assay. Nuclear extracts from the detached A549 and H157 cells were incubated with a specific CRE consensus sequence, and the activated CREB-CRE complex was quantified by phospho-CREB S133 ELISA.

(D) RNA levels of CREB transcription targets PTK6, ING3, and Fascin-1 in RSK2 and GDH1 knockdown cells were determined by quantitative RT-PCR.

(E) Effect of CREB phosphorylation-mimetic mutant S133D (SD) or -deficient mutant S133A (SA) expression on cell invasion and anoikis resistance in GDH1 and RSK2 knockdown cells. GDH1 and RSK2 double knockdown cells were overexpressed with myc-tagged CREB SD or SA mutants, and invasive and anoikis resistant potentials were determined by Matrigel cell invasion assay and annexin V staining.

(F) Effect of p38 or CREB inhibitors on p38 and CREB activity. A549 cells were treated with 5 μ M BIRB 796 (p38 inhibitor) or 100 nM 666–15 (CREB inhibitor) for 24 h. The activities of p38 and CREB were assessed by p38 T180/Y182 and CREB S133 phosphorylation.

(G and H) Effect of CREB S133D overexpression or 10 μ M of p38 activator U-46619 on cell invasion and anoikis resistance in fmk- and R162-treated cells. A549 cells were treated with CREB S133D and/or U-46619 for 24 h, and invasive and anti-anoikis potentials were determined as in (E). Western blot results shown are representative of four (B) and two (F) independent biological experiments. Error bars represent \pm SD from two replicates for (A) and three replicates for the others. p values were obtained by one-way ANOVA (ns, not significant; *0.01 < p < 0.05; **p < 0.01). See also Figures S2–S4.

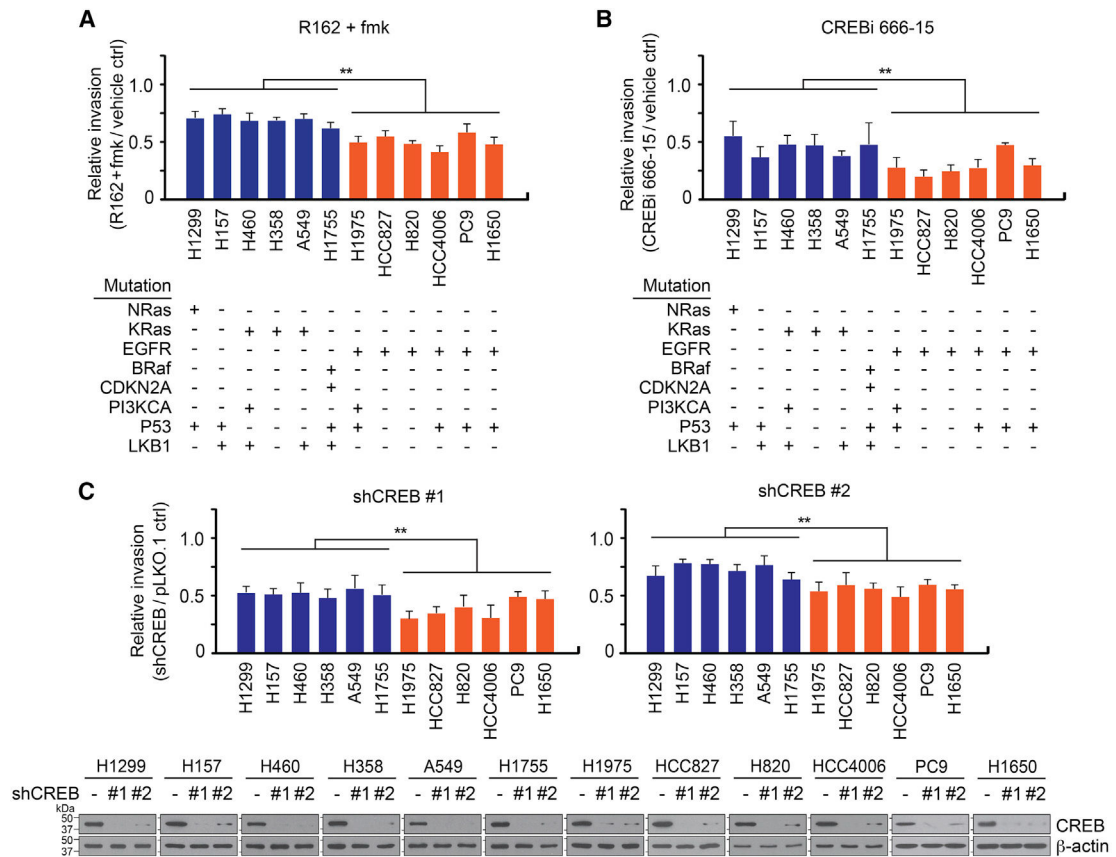


Figure 3. EGFR mutant-expressing lung cancer cells are more sensitive to GDH1/RSK2-CREB inhibition than cells with other oncogenic mutations

(A) Effect of RSK2 and GDH1 inhibition on cell invasion in lung cancer cell lines with different oncogenic mutations. Cell lines classified by genetic mutations were treated with fmk and R162 followed by invasion assay as described in Figure 1B. Cells with EGFR-activating mutations and inhibitor-resistant mutations are marked in orange.

(B and C) Effect of CREB inhibition on cell invasion of lung cancer cell lines with different oncogenic mutations. CREB was target downregulated using 100 nM of 666-15 (B) or CREB shRNA clones (C). Knockdown efficiency of CREB was assessed by immunoblotting. Error bars represent \pm SD from three replicates for (A)–(C). p values were obtained by two-tailed Student's t test for (A), (B), and (C) (**p < 0.01).

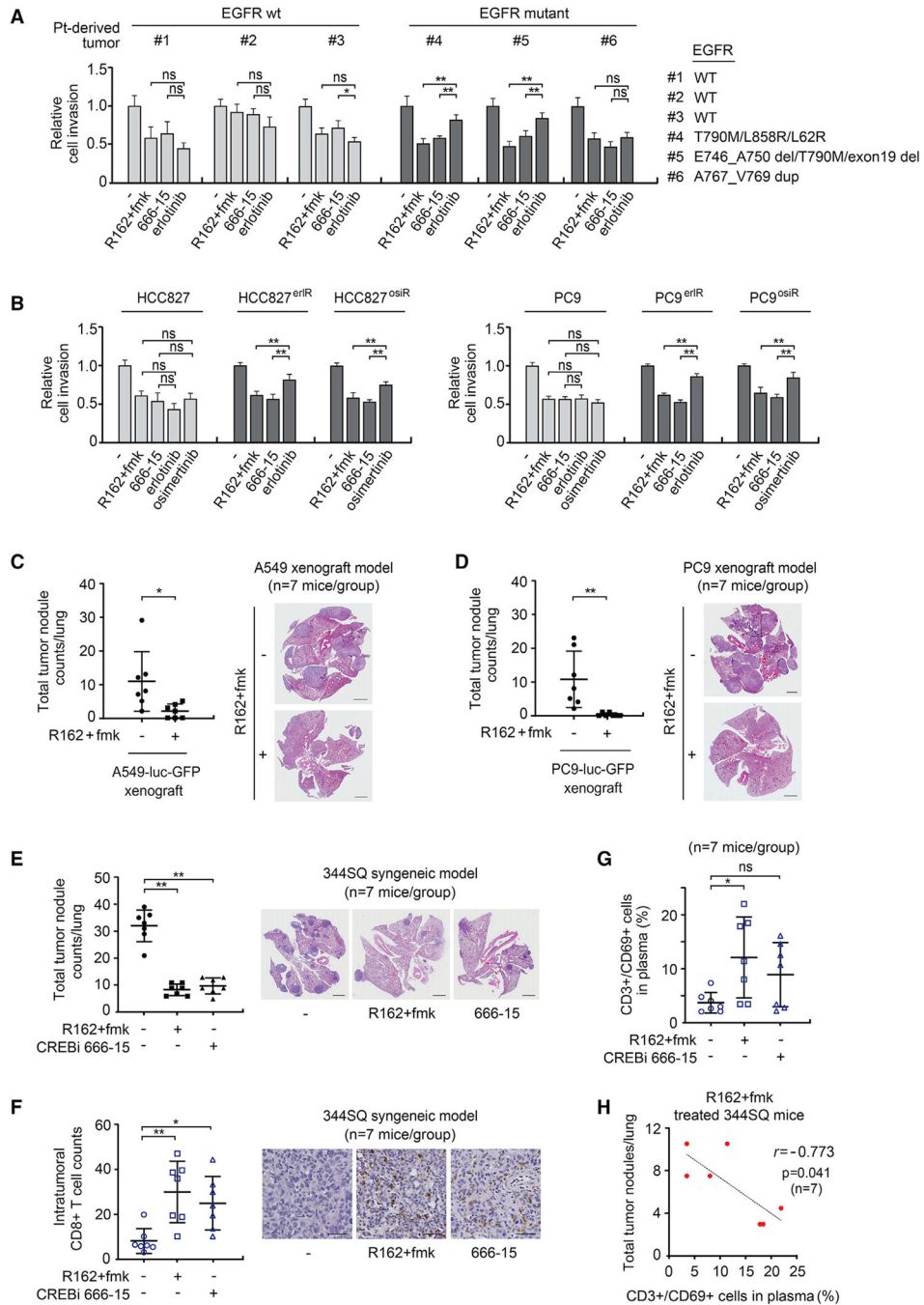


Figure 4. Inhibition of RSK2/GDH1-CREB effectively suppresses cell invasion, metastasis, and immune evasion in lung cancer including EGFR inhibitor-resistant tumors

(A) Invasion assay using NSCLC patient-derived tumors with or without EGFR mutations treated with inhibitors against RSK/GDH (5 μ M fmk/20 μ M R162), CREB (100 nM 666–15), or EGFR (1 μ M erlotinib).

(B) Parental, erlotinib^R, and osimertinib^R sets of HCC827 and PC9 cells with RSK/GDH, CREB, or EGFR inhibitor treatment were assayed for invasive potential. HCC827 and PC9 derivatives were treated with fmk/R162 and 666–15 as in (A) and 1 nM of erlotinib or osimertinib for 24 h followed by invasion assay.

(C and D) Effect of fmk and R162 combination on tumor metastasis in A549 (EGFR WT; C) and PC9 (EGFR mutant; D) xenograft mouse models. Mice were administered 20 mg/kg of R162 and 25 mg/kg of fmk for 14 weeks. Number of tumor nodules in the lungs (left) and representative H&E staining images (right) of each group are shown. Scale bars represent 2 mm.

(E) Effect of fmk/R162 or 666–15 on tumor metastasis in 344SQ syngeneic mouse model. Mice were administered 20 mg/kg of R162 and 25 mg/kg of fmk or 10 mg/kg of 666–15 for 29 days. Number of tumor nodules in the lungs and representative H&E staining images are shown. Scale bars represent 2 mm.

(F and G) Number of CD8+ T cells in tumors (F) or percentage of activated T cells in plasma (G) of 344SQ model shown in (E). CD8+ T cells in tumors were IHC stained, and representative images are shown on the right. Scale bars represent 50 μ m for (F). Activated T cells in plasma were quantified by CD3 and CD69 dual positivity.

(H) Correlation between tumor nodules and activated T cells in mice shown in (E)–(G). Error bars represent \pm SD from four (A) and three (B) replicates. (C)–(H) are from seven mice for each group. p values were determined by one-way ANOVA for (A), (B), and (E)–(G) and unpaired Student's t test for (C) and (D). Pearson's correlation coefficient was used for (H) (ns, not significant; *0.01 < p < 0.05; **p < 0.01). See also Table S2 and Figures S5 and S6.

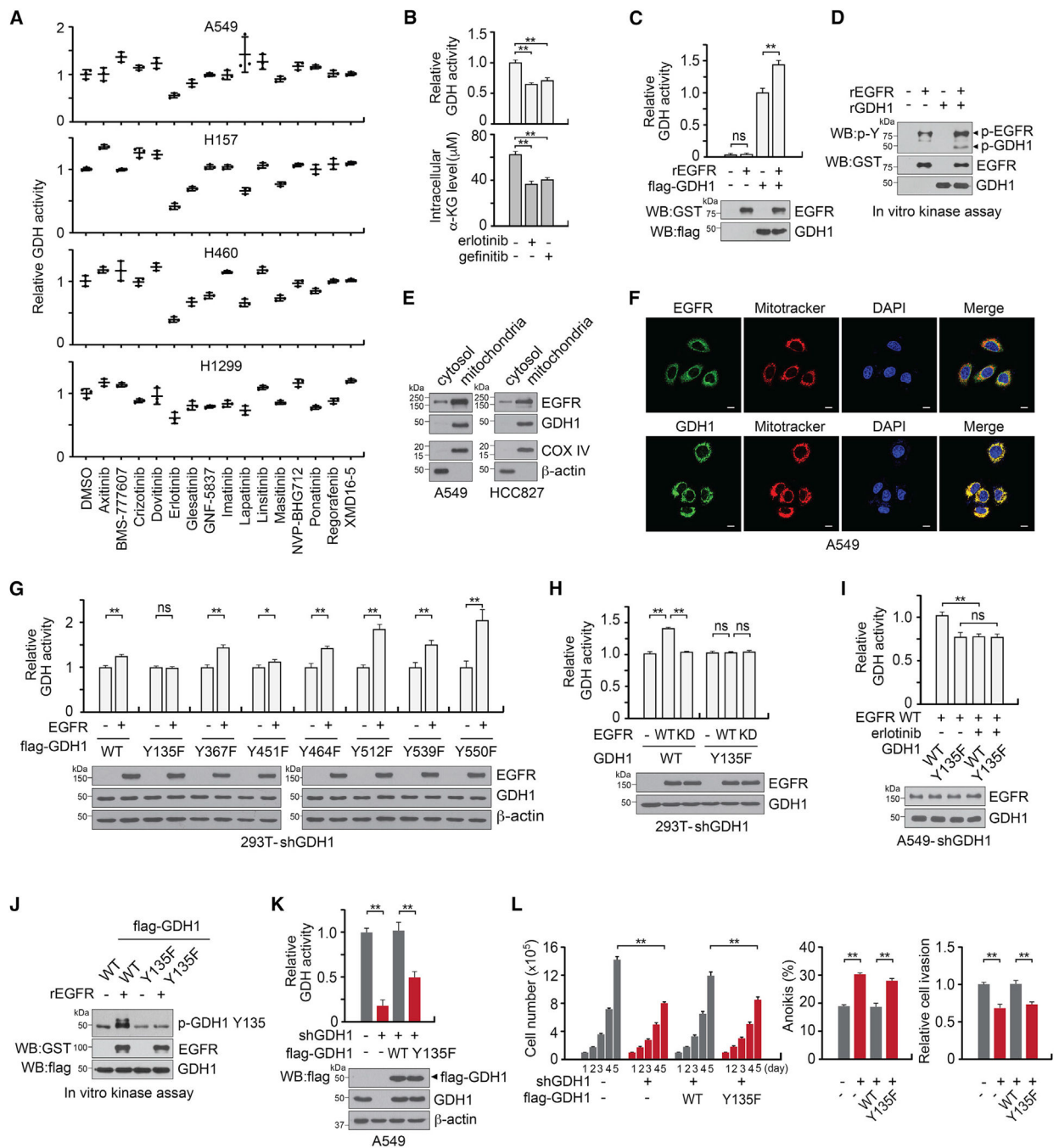


Figure 5. EGFR phosphorylates GDH1 at Y135 and enhances GDH activity in cancer cells

(A) Profiling of oncogenic kinase inhibitor effect on GDH activity in lung cancer cells. Cells were treated with 10 μ M drugs for 4 h, and GDH activity was assessed.

(B) Effect of EGFR inhibition on GDH activity and intracellular α -KG levels. A549 cells were treated with 10 μ M of erlotinib or gefitinib for 4 h followed by α -KG and GDH activity assays.

(C) Effect of EGFR on GDH activity by *in vitro* coupled enzyme assay. *In vitro* EGFR kinase assay was performed using recombinant active EGFR and flag-GDH1 followed by GDH1 activity assay.

(D) *In vitro* kinase assay was performed using recombinant EGFR and GDH1. Phosphorylation of GDH1 was detected by immunoblotting using pan-phospho-Tyr antibody.

(E) Western blot analysis showing the cytosolic and mitochondrial localization of EGFR and GDH1 in lung cancer cells. β -actin and Cox IV were used as markers for cytosol and mitochondria, respectively.

(F) Immunofluorescence assay shows the localization of EGFR and GDH1 with MitoTracker in A549 cells. Scale bars represent 10 μ m.

(G) Phosphorylation at Y135, but not others, by EGFR leads to enhanced GDH1 activity. 293T cells with endogenous GDH1 knockdown were transfected with EGFR and GDH1 variants, and GDH activity was measured.

(H and I) EGFR-induced GDH1 activation is mediated by Y135 GDH phosphorylation. EGFR wild-type (WT) or kinase dead (KD) mutant was expressed (H) or 10 μ M erlotinib was treated (I) in cells expressing GDH1 WT or Y135F.

(J) *In vitro* EGFR kinase assay using GDH1 variants as substrates. Phosphorylation at Y135 of GDH1 was detected by immunoblotting using specific antibody against phospho-Y135 GDH1.

(K and L) Effect of GDH1 phosphorylation on GDH activity (K), proliferation, anoikis induction, and cell invasion (L). GDH activity assay, trypan blue staining, anoikis assay, and Matrigel invasion assay were performed using A549 cells with GDH1 knockdown and GDH1 WT or Y135F expression. Western blot results shown are representative of two (D and J) and three (E) independent biological experiments. Error bars represent \pm SD from three replicates. p values were determined by two-tailed Student's t test for (G) and one-way ANOVA for the rest. (ns, not significant; *0.01 < p < 0.05; **p < 0.01). See also Figure S7.

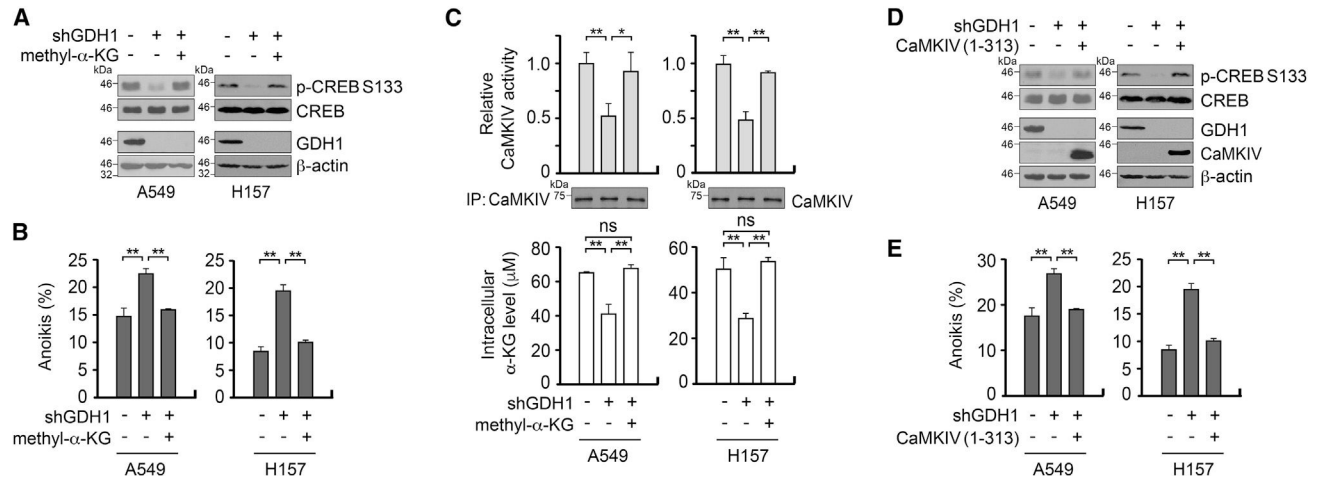


Figure 6. GDH1 and its product α -KG promote CREB activity through CaMKIV

(A and B) Rescue effect of α -KG on CREB activity and anoikis resistance in cells with GDH1 knockdown. Detached cells were treated with dimethyl- α -KG for 48 h, and the activity of CREB (A) and anoikis (B) was assessed by phospho-CREB S133 immunoblotting and annexin V staining, respectively.

(C) CaMKIV activity in GDH1 knockdown A549 or H157 cells in the presence and absence of α -KG. Cells were cultured on 1% agarose for 48 h with or without dimethyl- α -KG (A549: 5 mM, H157: 1 mM). Top: endogenous CaMKIV was immunoprecipitated and kinase activity was assessed using synthetic peptide substrate of CaMKIV as a substrate. Bottom: intracellular α -KG levels were measured using cell lysates.

(D and E) Rescue effect of a constitutively active mutant form of CaMKIV on CREB activity and anoikis resistance in GDH1 knockdown cells. GDH1 knockdown cells were transiently transfected with CaMKIV (1–313), and CREB activity was determined by phospho-CREB S133 (D), and anoikis was assessed by annexin V staining (E). Western blot results shown are representative of two independent biological experiments for (A) and (D). Error bars represent \pm SD from three replicates. p values were obtained by one-way ANOVA (ns, not significant; *0.01 < p < 0.05; **p < 0.01).

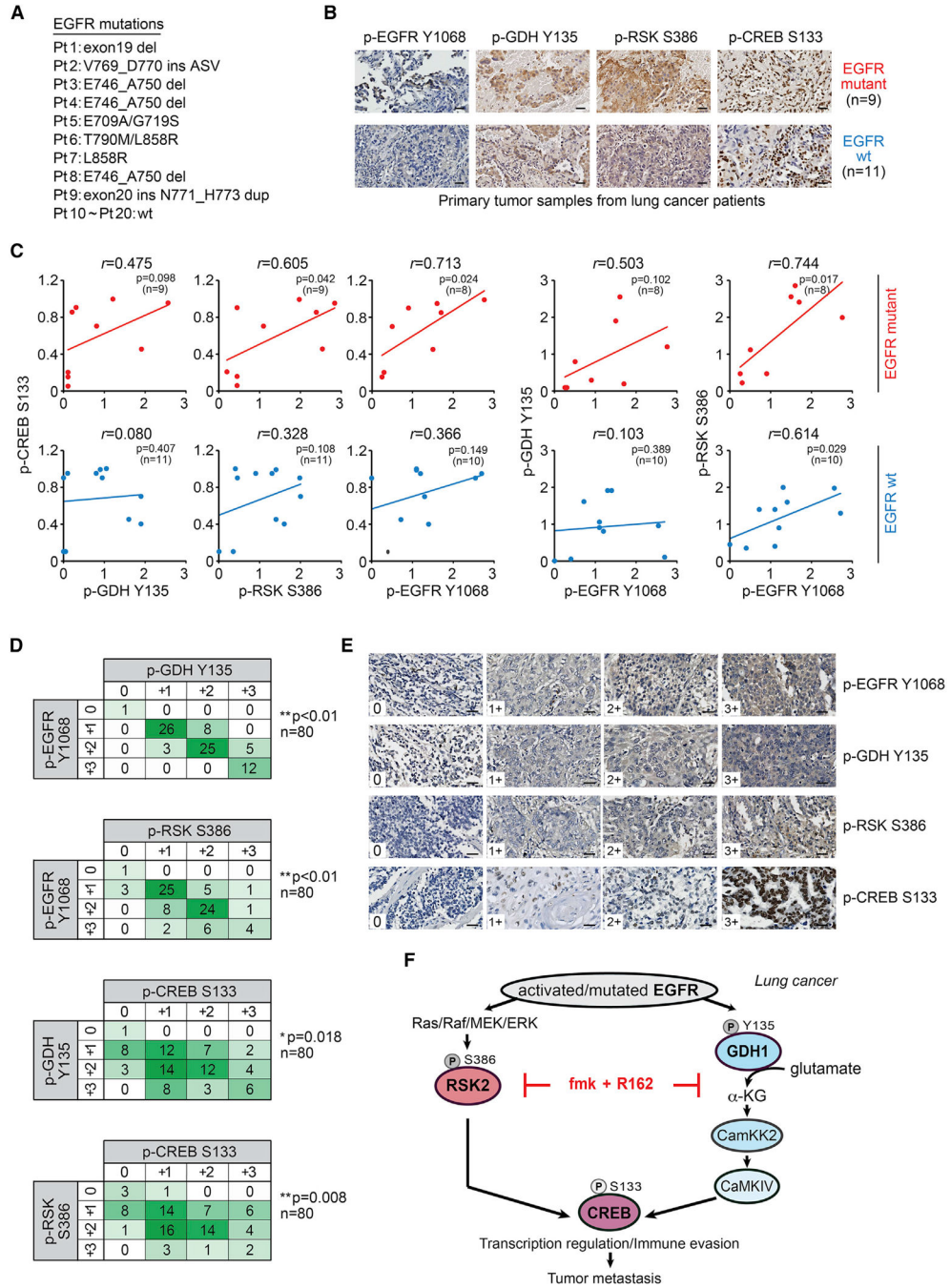


Figure 7. Phosphorylation and activation of EGFR, GDH1, or RSK2 and CREB correlate more evidently in human lung cancer with EGFR mutations

(A–C) Immunohistochemistry (IHC) analyses of phospho-EGFR Y1068, GDH Y135, RSK S386, and CREB S133 using primary tumor tissues from lung cancer patients with EGFR WT (n = 9) or mutations (n = 11). EGFR mutational status (A), representative images for each group (B), and the correlation between phosphorylated CREB, GDH, RSK, and EGFR in EGFR mutant (top) and EGFR WT (bottom) (C) are shown. Staining positivity ratio (0–1) and intensity (0~+3) were scored. Patient (Pt) 9 and 20 tumors were not stained for p-EGFR due to limited specimen collection.

(D and E) IHC analyses of phosphorylation at EGFR Y1068, GDH Y135, RSK S386, and CREB S133 in metastatic lung cancer patients (US Biomax; n = 80/group). The correlations between p-EGFR Y1068, p-GDH Y135, p-RSK S386, and p-CREB S133 (D) and representative IHC images for 0, +1, +2, and +3 scores (E) are shown. Scale bars represent 50 μm in (B) and (E). Pearson's correlation coefficient (C) and Chi-square test (D) were used for statistical analyses.

(F) Proposed model of co-targeting GDH1 and RSK2 in EGFR-mutated lung cancer. Mutated and activated EGFR phosphorylates GDH1 at Y135 to promote transcriptional activity of CREB through CaMKIV. Mutated EGFR activates RSK2 through the Ras/Raf/MEK/ERK pathway, which consequently phosphorylates CREB and contributes to its activation. Combined targeting of GDH1 and RSK2 is effective in attenuating cancer progression driven by EGFR mutation and activation. See also Figure S7 and Table S2.

KEY RESOURCES TABLE

REAGENT or RESOURCE	SOURCE	IDENTIFIER
Antibodies		
Rabbit polyclonal anti-GDH1 antibody	Abcam	Cat#ab89967; RRID: AB_2263346
Mouse monoclonal anti-RSK2 (clone E-1) antibody	Santa Cruz Biotechnology	Cat#sc-9986; RRID: AB_672176
Mouse monoclonal anti-beta-actin (clone AC-74) antibody	Sigma-Aldrich	Cat#A2228; RRID: AB_476697
Rabbit monoclonal anti-phospho-CREB Ser133 (clone 87G3) antibody	Cell Signaling Technology	Cat#9198; RRID: AB_2561044
Rabbit monoclonal anti-CREB (clone 48H2) antibody	Cell Signaling Technology	Cat#9197; RRID: AB_331277
Rabbit monoclonal anti-phospho-AKT Ser473 (clone D9E) antibody	Cell Signaling Technology	Cat#4060; RRID: AB_2315049
Mouse monoclonal anti-AKT1 antibody (clone 2H10) antibody	Cell Signaling Technology	Cat#2967; RRID: AB_331160
Rabbit monoclonal anti-phospho-ERK1/2 Thr202/Tyr204 (clone 20G11) antibody	Cell Signaling Technology	Cat#4376; RRID: AB_331772
Rabbit monoclonal anti-ERK1/2 (clone 137F5) antibody	Cell Signaling Technology	Cat#4695; RRID: AB_390779
Mouse monoclonal anti-Myc tag (clone 9B11) antibody	Cell Signaling Technology	Cat#2276; RRID: AB_331783
Mouse monoclonal anti-phospho-p38 Thr180/Tyr182 (clone 28B10) antibody	Cell Signaling Technology	Cat#9216; RRID: AB_331296
Rabbit polyclonal anti-p38 antibody	Cell Signaling Technology	Cat#9212; RRID: AB_330713
Rabbit monoclonal anti-CD8 alpha (clone EPR21769) antibody	Abcam	Cat#ab217344; RRID: AB_2890649
FITC-anti-mouse monoclonal CD3 (clone 17A2) antibody	BioLegend	Cat#100204; RRID: AB_312661
PE-anti-mouse monoclonal CD69 (clone H1.2F3) antibody	BioLegend	Cat#104508; RRID: AB_313111
Mouse monoclonal anti-glutathione S-transferase (clone GST-2) antibody	Sigma Aldrich	Cat#G1160; RRID: AB_259845
Mouse monoclonal anti-FLAG (clone M2) antibody	Sigma Aldrich	Cat#F3165; RRID: AB_259529
Mouse monoclonal anti-phospho-Tyr (clone PY99) antibody	Santa Cruz Biotechnology	Cat#sc-7020; RRID: AB_628123
Rabbit monoclonal anti-EGFR (clone D38B1) antibody	Cell Signaling Technology	Cat#4267; RRID: AB_2246311
Rabbit monoclonal anti-Cox IV (clone 3E11) antibody	Cell Signaling Technology	Cat#4850; RRID: AB_2085424
Rabbit polyclonal anti-phospho-Tyr135 GDH1 antibody	Shanghai Genomics	N/A
Anti-rabbit IgG Alexa Fluor 488 antibody	Invitrogen	Cat#A11070; RRID: AB_2534114
Rabbit polyclonal anti-CaMKIV antibody	Cell Signaling Technology	Cat#4032; RRID: AB_2068389
Rabbit polyclonal anti-phospho-RSK2 Ser386 antibody	Cell Signaling Technology	Cat#9341; RRID: AB_330753
Rabbit monoclonal anti-phospho-EGFR Tyr1068 (clone D7A5) antibody	Cell Signaling Technology	Cat#3777; RRID: AB_2096270
Rabbit polyclonal anti-IFN gamma antibody	Proteintech	Cat#15365-1-AP; RRID: AB_2123037
Rabbit monoclonal anti-LKB1 (clone D60C5F10) antibody	Cell Signaling Technology	Cat#13031; RRID: AB_2716796
Biological samples		
Lung cancer patient-derived xenografts tumors	The Jackson Laboratory	Cat#TM01446, TM00302, TM00186, TM01244, TM00219, J000100672
Human lung cancer tissue microarray	US Biomax	Cat#LC817b
Human lung tumor tissues	This paper	N/A
Chemicals, peptides, and recombinant proteins		

REAGENT or RESOURCE	SOURCE	IDENTIFIER
Polydatin	Santa Cruz Biotechnology	Cat#sc-203203; CAS: 65914-17-2
A922500	Selleckchem	Cat#S2674; CAS: 959122-11-3
ATIC Dimerization Inhibitor	Sigma Aldrich	Cat#118490; CAS: 1402453-15-9
R162	Sigma Aldrich	Cat#R162205; CAS: 64302-87-0
Lometrexol	Cayman	Cat#18049; CAS: 106400-81-1
PFKFB3 Inhibitor, 3PO	Sigma Aldrich	Cat#525330; CAS: 18550-98-6
Triparanol	Sigma Aldrich	Cat#T5200; CAS: 78-41-1
Methotrexate	Sigma Aldrich	Cat#A6770; CAS: 133073-73-1
Brequinar	Selleckchem	Cat#S6626; CAS: 96187-53-0
Clorgyline	MedChemExpress	Cat# HY-14197A; CAS:17780-75-5
Malic enzyme inhibitor, ME1	MedChemExpress	Cat#HY-124861; CAS: 522649-59-8
L-Buthionine-(S,R)-Sulfoximine, BSO	Cayman	Cat# 14484; CAS: 83730-53-4
RO48-8071 fumarate	MedChemExpress	Cat#HY-18630A; CAS: 189197-69-1
2,4-Diamino-6-hydroxypyrimidine, DAHP	Selleckchem	Cat#S3688; CAS: 56-06-4
fmk	MedChemExpress	Cat#HY-52101A; CAS: 821794-92-7
BI-D1870	Selleckchem	Cat#S2843; CAS: 501437-28-1
LJI308	Selleckchem	Cat#S7871; CAS: 1627709-94-7
BPTES	Selleckchem	Cat#S7753; CAS: 314045-39-1
EGCG	Selleckchem	Cat#S2250; CAS: 989-51-5
666-15	Sigma Aldrich	Cat#5383410001
Erlotinib	Selleckchem	Cat#S7786; CAS: 183321-74-6
Osimertinib	Selleckchem	Cat#S7297; CAS: 1421373-65-0
BIRB 796	Selleckchem	Cat#S1574; CAS: 285983-48-4
U-46619, P38 activator	Santa Cruz Biotechnology	Cat#sc-201242; CAS: 56985-40-1
Axitinib	Selleckchem	Cat#S1005; CAS: 319460-85-0
BMS-777607	Selleckchem	Cat#S1561; CAS: 1025720-94-8
Crizotinib	Selleckchem	Cat#S1068; CAS: 877399-52-5
Dovitinib	Selleckchem	Cat#S1018; CAS: 405169-16-6
Glesatinib	MedChemExpress	Cat#HY-19642; CAS: 936694-12-1
GNF-5837	Selleckchem	Cat#S7519; CAS: 1033769-28-6
Imatinib	Selleckchem	Cat#S2475; CAS: 152459-95-5
Lapatinib	Selleckchem	Cat#S2111; CAS: 231277-92-2
Linsitinib	Selleckchem	Cat#S1091; CAS: 867160-71-2
Masitinib	Selleckchem	Cat#S1064; CAS: 790299-79-5
NVP-BHG712	Selleckchem	Cat#S2202; CAS: 940310-85-0
Ponatinib	Selleckchem	Cat#S1490; CAS: 943319-70-8
Regorafenib	Selleckchem	Cat#S1178; CAS: 755037-03-7
XMD16-5	Selleckchem	Cat#S8273; CAS: 345098-78-3
MitoTracker Red	Invitrogen	Cat#M7512
CM-H2DCFDA	Invitrogen	Cat#C6827
Antifade mountant with DAPI	Invitrogen	Cat#P36931
Purified GDH1 from bovine liver	Sigma Aldrich	Cat#G2626

REAGENT or RESOURCE	SOURCE	IDENTIFIER
Recombinant EGFR	Invitrogen	Cat# PV4879
Dimethyl-alpha-ketoglutarate	Sigma Aldrich	Cat#75890; CAS: 13192-04-6
GDH1 Y135 peptides - SWEVIEG(p) YRAQHS	GenScript	Cat# U643JGA070
D-Luciferin	Perkin Elmer	Cat#122799; CAS: 2591-17-5
Matrigel Basement Membrane Matrix	Corning	Cat#354263
SYBR Green Master Mix	Bio-Rad	Cat#1725270
Dialyzed Fetal Bovine Serum	Sigma-Aldrich	Cat#F0926
Critical commercial assays		
FITC Annexin V Apoptosis Detection Kit	BD Biosciences	Cat#556547
CellTiter-Glo Luminescent Viability Assay	Promega	Cat#G7570
Human Phosphorylation Pathway Profiling Array C55	RayBiotech	Cat#AAH-PPP-1-4
ADP-Glo Kinase Assay	Promega	Cat#V6930
Alpha-ketoglutarate Assay	Abcam	Cat#ab83431
High-Capacity cDNA Reverse Transcription Kit	Applied Biosystems	Cat#4368814
CREB (Phospho-Ser133) Transcription Factor Assay	Cayman Chemical	Cat#10009846
Mouse ALT ELISA Kit	Abcam	Cat#ab282882
MILLIPLEX Mouse Kidney Toxicity Multiplex Assay	Sigma Aldrich	Cat#MKI2MAG-94K
Ammonia Assay Kit	Abcam	Cat#ab83360
Glutamine/Glutamate-Glo assay	Promega	Cat#J8021
ATP bioluminescent somatic cell assay kit	Sigma Aldrich	Cat#11699709001
NE-PER Nuclear and Cytoplasmic Extraction Reagents	Thermo Scientific	Cat#78833
Mitochondria Isolation Kit	Thermo Scientific	Cat#89874
Experimental models: Cell lines		
Human: MRC-5 cells	ATCC	Cat#CCL-171; RRID: CVCL_0440
Human: BEAS-2B cells	ATCC	Cat#CRL-9609; RRID: CVCL_0168
Human: H1299 cells	ATCC	Cat#CRL-5803; RRID: CVCL_0060
Human: H157 cells	ATCC	Cat#CRL-5802; RRID: CVCL_0463
Human: H460 cells	ATCC	Cat# HTB-177; RRID: CVCL_0459
Human: H358 cells	ATCC	Cat#CRL-5807; RRID: CVCL_1559
Human: A549 cells	ATCC	Cat#CCL-185; RRID: CVCL_0023
Human: H1755 cells	ATCC	Cat#CRL-5892; RRID: CVCL_1492
Human: H1975 cells	ATCC	Cat#CRL-5908; RRID: CVCL_1511
Human: HCC827 cells	ATCC	Cat#CRL-2868; RRID: CVCL_2063
Human: H820 cells	ATCC	Cat#HTB-181; RRID: CVCL_1592
Human: HCC4006 cells	ATCC	Cat#CRL-2871; RRID: CVCL_1269
Human: PC9 cells	Sigma Aldrich	Cat#90071810; RRID: CVCL_1640
Human: H1650 cells	ATCC	Cat#CRL-5883; RRID: CVCL_1483
Murine: 344SQ cells	Gibbons et al. ³³	N/A
Murine: LLC1 cells	ATCC	Cat#CRL-1642; RRID: CVCL_4358

REAGENT or RESOURCE	SOURCE	IDENTIFIER
Experimental models: Organisms/strains		
Mouse: Hsd:Athymic Nude-Foxn1nu	Envigo	Cat#069
Mouse: 129S1/SvImj	The Jackson Laboratory	Cat#002448
Mouse: C57BL/6JOLA-Hsd	Envigo	Cat#057
Oligonucleotides		
shRNA targeting sense sequence: RSK2 #1: CGCTGAGAATGGACAGCAAAT	Horizon Discovery	Cat#TRCN0000040144
shRNA targeting sense sequence: RSK2 #2: GCCTGAAGATACATTCTATTT	Horizon Discovery	Cat#TRCN0000040147
shRNA targeting sense sequence: GDH1 #1: GCCATTGAGAAAGTCTTCAAA	Horizon Discovery	Cat#TRCN0000028600
shRNA targeting sense sequence: GDH1 #2: CCCAAGAACTATACTGATAAT	Horizon Discovery	Cat#TRCN0000028588
shRNA targeting sense sequence: CREB #1: GCTCGATAAATCTAACAGTTA	Horizon Discovery	Cat#TRCN0000007308
shRNA targeting sense sequence: CREB #2: CGTCTAATGAAGAACAGGGAA	Horizon Discovery	Cat#TRCN0000007310
Primer: Fascin-1 Forward AGCCAGGGGCGGGACA	Integrated DNA Technologies	N/A
Primer: Fascin-1 Reverse CGCTCCACAAAGCCCAGCTA	Integrated DNA Technologies	N/A
Primer: PTK6 Forward TGCTCTGGAGCGCCTGT	Integrated DNA Technologies	N/A
Primer: PTK6 Reverse TGTGGCCCAGCTGGAGCA	Integrated DNA Technologies	N/A
Primer: ING3 Forward AGAAAACACTATTCCCACAGAGG	Integrated DNA Technologies	N/A
Primer: ING3 Reverse AAAAAAAACCACTTTGGCGCCTGAG	Integrated DNA Technologies	N/A
Primer: GAPDH Forward GACATCAAGAAGGTGGTG	Integrated DNA Technologies	N/A
Primer: GAPDH Reverse GTCATACCAGGAAATGAGC	Integrated DNA Technologies	N/A
Recombinant DNA		
Plasmid: Gateway pDEST27	Invitrogen	Cat#11812013
Plasmid: pLHCX	Takara	Cat#631511
Plasmid: pMSCV-hyg-Gateway	This paper	N/A
Plasmid: pRSV-CaMKIV (1-313)	Sun et al. ³⁵	Addgene plasmid: pRSV-CaMKIV(1-313); Cat#45063
Plasmid: pHAGE PGK-GFP-IRES-LUC-W	Wilson et al. ⁴⁰	Addgene plasmid: pHAGE PGK-GFP-IRES- LUC-W; Cat#46793
Plasmid: pBabe-puro-EGFR WT	Greulich et al. ⁴¹	Addgene plasmid: EGFR WT; Cat#11011
Plasmid: pBabe-puro-EGFR D837A	Greulich et al. ⁴¹	Addgene plasmid: EGFR D837A; Cat#11014
Plasmid: pMSCV-myc-CREB S133D	This paper	N/A
Plasmid: pMSCV-myc-CREB S133A	This paper	N/A
Plasmid: pLHCX-flag-GDH1 WT	This paper	N/A

REAGENT or RESOURCE	SOURCE	IDENTIFIER
Plasmid: pLHCX-flag-GDH1 Y135F	This paper	N/A
Software and algorithms		
CompuSyn software	ComboSyn Inc.	https://www.combosyn.com/
ImageJ software	National Institutes of Health	https://imagej.nih.gov/ij/
GraphPad Prism software	GraphPad Software	http://www.graphpad.com
Clinical annotation related to Figure 7	US Biomax	http://www.biomax.us

Author Manuscript

Author Manuscript

Author Manuscript

Author Manuscript